

**An Observational Study of the Interactions
Between the Seasonal Mean Flow
and the Transient Eddies**

Jian Sheng and Jacques Derome

CRG Report No. 89-15

October, 1989

An Observational Study of the Interactions
Between the Seasonal Mean Flow and the Transient Eddies

Jian Sheng
and
Jacques Derome

Department of Meteorology
McGill University
805 Sherbrooke Street West
Montréal, Québec
Canada, H3A 2K6

October 1989

ABSTRACT

The large-scale energetics of the Northern Hemisphere atmospheric motions are spectrally analysed in the frequency domain using a five-year data set from the ECMWF operational analyses. The geographical distributions of kinetic energy (KE) of the fast transients (periods shorter than 10 days) assume the shape of elongated bands indicating the storm track structure. The slow transients (periods longer than 10 days) exhibit local maxima of KE in the eastern parts of the major oceans. The slow transient available potential energy (APE), on the other hand, has maxima over the American and Asian continents.

The baroclinic conversion is the dominant energy source responsible for the maintenance of the low frequency disturbances when hemispherically integrated quantities are considered. The barotropic and nonlinear conversions, on the other hand, provide important local contributions to the KE of the slow transients.

With the flow separated in terms of three frequency "bands", namely, the seasonal mean, the low and the high frequency eddies, the energy cycle is a rather simple one. In summer, i) the APE flows from the lower to higher frequency bands, ii) the baroclinic conversion transforms APE to KE for all frequency bands and finally, iii) KE flows from higher to lower frequencies (including the time-mean flow). In winter, the energy flows in the same direction, except for one transfer, the exchange of KE between the time-mean rflow and the slow transients. The directions is from the time-mean flow to the slow transients, presumably because the time-mean motions are barotropically unstable in winter.

1. Introduction

In recent papers by Sheng and Hayashi (1989a, b), the atmospheric energetics were studied spectrally in the frequency domain with a focus on the energy balance of low frequency disturbances. To study the energy cycle in terms of kinetic energy (KE) and available potential energy (APE), they divided the transient fluctuations into low frequency and high frequency (synoptic time scale) groups with a dividing period of 10 days. The choice of the 10-day period is related to the fact that eddies with periods longer than 10 days gain KE (lose APE) while those with periods shorter than 10 days lose KE (gain APE) from exchanges with other frequencies. It was shown that the energy balance for the low frequency transients is quite different from that for the high frequency ones. Transients of the synoptic time scale are energetically typical of those predicted by the baroclinic instability theory (Charney 1947, Eady 1949), i.e., the time-mean APE is first converted into synoptic scale APE, and then into transient KE. The maintenance of low frequency transients, however, is complicated by the fact that, although the baroclinic energy conversion is the major KE source, nonlinear exchanges of KE between the slow and fast transients also play an important role. Data analyses, both from atmospheric observations and from general circulation models (GCMs), indicate a systematic flow of KE from high frequency bands to the low frequency bands. This kind of energy decascade is reminiscent of the nonlinear energy exchange in the wavenumber domain (Saltzman 1970, Chen and Wiin-Nielsen, 1978).

Simmons et al. (1983) proposed a theory for the existence of low frequency transient variability. In a linear stability analysis of a barotropic

model with a realistic zonally and meridionally varying wintertime basic state, the most rapidly growing modes were found to be those related to the observed "Pacific/North American" and "East Atlantic" teleconnection patterns. The mechanism by which the slow transients extract kinetic energy from the time-mean flow is through the down-gradient flow of zonal momentum in the jet-exit regions. It is, therefore, a two-dimensional barotropic instability with a fundamental difference from the classical theory of a zonally symmetric barotropic jet (Kuo, 1949). Wallace and Lau (1985) tested this concept with several observational data sets for the Northern Hemisphere wintertime. In a systematic analysis of the structure and horizontal distributions of eddy transients for the high and low frequency bands, they positively identified the importance of barotropic instability in the generation of slow transients. It was shown that the winter time-mean flow at the 300mb level barotropically supplies KE to the low frequency transients, but extracts KE from the high frequency disturbances.

In the energy calculations of Sheng and Hayashi (1989a, b), however, the barotropic conversion of kinetic energy between the time-mean flow and the transient eddies is less instrumental. The transient eddies supply only a small amount of KE (small in comparison with the baroclinic conversion) to the time-mean flow in both the high and low frequency ranges. The analyses of Sheng and Hayashi used multi-level data sets and more complete equations than those of Wallace and Lau. On the other hand, the fundamental difference between the two studies is perhaps due to the use of an annual mean flow in Sheng and Hayashi rather than a wintertime mean as in Wallace and Lau. The first purpose of this study is therefore to recalculate the energetics in the frequency domain for the winter and summer seasons separately and con-

trast the results, in the hope of giving a more comprehensive view of the energetics of the slow transients.

In most earlier works (e.g., Lorenz, 1967), general circulation statistics were presented in a zonally averaged format, which precludes any study of longitudinal differences. In more recent studies (e.g., Blackmon et al., 1977), analyses were extended longitudinally and some emphasis was placed on examining the longitudinal distributions of the contributions to the energy integrals. The results clearly illustrated that general circulation statistics exhibit strong longitudinal variations and geographical patterns. The latitude-pressure cross-sections of energy parameters were discussed in Sheng and Hayashi (1989b). It is very interesting that the direction of non-linear KE exchange reverses its sign from the mid-latitudes to the tropics. Instead of being enhanced, the slow transients are actually damped by the fast transients in the low latitudes. To further explore the processes responsible for the existence of slow transients, the geographical distributions of energetics in the frequency domain are studied in this paper.

In Section 2 the scheme and data set in this study are briefly reviewed. The contrast of hemispherically integrated energetics between the winter and summer seasons is discussed in Section 3. The geographical distributions of energy and energy conversion terms are presented in Sections 4 and 5, for the winter and summer seasons, respectively. The results are summarized in Section 6.

2. Energy equations in the frequency domain and data analysis procedure

The form of spectral energy equations in the frequency domain used in this study is a variation of those discussed in Hayashi (1980) and Sheng and Hayashi (1989a). The formulation invokes the use of the cross-spectral technique to compute the nonlinear advection and curvature terms in the governing equations. In comparison with the conventional method of convolution in the frequency domain, the scheme effectively reduces the amount of calculations involved. The KE and APE equations in the frequency domain can be written as,

$$LK^{\ell} + NK^{\ell} + AK^{\ell} + FK^{\ell} + FP^{\ell} - D^{\ell} = 0, \quad (1)$$

$$LK^h + NK^h + AK^h + FK^h + FP^h - D^h = 0, \quad (2)$$

$$LA^{\ell} + NA^{\ell} - AK^{\ell} + FA^{\ell} + G^{\ell} = 0, \quad (3)$$

$$LA^h + NA^h - AK^h + FA^h + G^h = 0. \quad (4)$$

Here the superscripts ℓ and h denote the energy transfer terms for the low and high frequency bands, respectively. The various terms in Eqs (1) through (4) are interpreted as follows:

AK baroclinic conversion from APE to KE

D dissipation of transient KE

FA convergence of transient APE flux

FK convergence of transient KE flux

FP convergence of transient flux of potential energy

G generation of transient APE

LA transfer of APE from the time-mean flow into the transient eddies

LK transfer of KE from the time-mean flow into the transient eddies

NA transfer of APE due to nonlinear interactions of transient eddies

NK transfer of KE due to nonlinear interactions of transient eddies

The mathematical expression for each term is given in Appendix A and a list of symbols used in the above equations can be found in Appendix B.

The data set used in this study is from the operational analyses of the European Centre for Medium Range Weather Forecasts (ECMWF). From the original data set, we extracted the geopotential height and temperature at the 100mb, 200mb, 300mb, 500mb, 700mb, 850mb, and 1000mb pressure levels, on a 5-degree longitude-latitude mesh, at 24-hour intervals. The period starts at 12 GMT January 1, 1980 and ends at 12 GMT December 31, 1984. The same data were used by Sheng and Hayashi (1989b). The vertical velocity is calculated kinematically from the continuity equation with values of calculated horizontal divergence corrected by the method suggested by O'Brien (1970). The time-mean flow is defined as the 120-day time average, starting from November 16 for the winter season, and from May 16 for the summer season. The seasonal variation has been excluded from the transient flow by removing the first four Fourier harmonics of the annual cycle from all the time series, following Blackmon et al. (1977). Hence the frequency range of our analysis corresponds to periods between about 2 and 90 days. Due to the lack of direct measurements of diabatic heating and dissipation in the atmosphere, the G and D terms in Eqs (1) through (4) are computed as residuals required for an assumed balance.

3. A comparison of energetics between the summer and the winter seasons

The distributions of KE, APE and AK in the frequency domain are shown in Figs 1, 2 and 3 for the winter and the summer seasons. The abscissa corresponds to frequency bands in constant interval of log-frequency, and the ordinate indicates the spectra integrated in that band. The advantage of this presentation has been discussed in Sheng and Hayashi (1989a). All the values have been averaged over the entire mass of the Northern Hemisphere, and the units are in J/m^2 for APE and KE, and in W/m^2 for the energy conversion terms.

The distribution of KE is characterized by a pronounced energy concentration at the mean flow. About 61 percent in winter, and 44 percent in summer, of the total KE is time independent (Fig. 1a and Fig. 1b). On the other hand, a broad maximum occurs at the high frequency region, for both seasons. These features are consistent with the results of Sheng and Hayashi (1989a). Presented in Fig. 1c is the spectral KE calculated from the yearly data which include all 12 months in the time series. It is easy to see that by removing the seasonal cycle, as described in Section 2, the energy level in the low frequency range is significantly reduced, but is virtually unchanged at the high frequency end.

A comparison of Figs 1, 2 and 3 indicates that the levels of KE, APE and AK at all frequency bands are higher in winter than in summer. However, the low frequency transients appear to experience a relatively moderate annual oscillation in comparison with the high frequency eddies. It is understood that the strong seasonal contrast of high frequency transient activity is closely related to the seasonal contrast of baroclinicity in the atmos-

where: strong disturbances in the wintertime are a direct consequence of stronger vertical wind shears and horizontal temperature gradients in the troposphere. Therefore a weaker dependence of slow transients upon baroclinicity is suggested. Another interesting observation is the frequency shift of energy peaks between the two seasons. In the wintertime (Fig. 1a and 2a), both KE and APE peak at higher frequencies than in the summertime (Fig. 1b and 2b). This could be explained by the stronger westerlies in the cold season. Due to the effect of horizontal advection, the majority of eastward-moving disturbances tend to speed up in the wintertime, and therefore more energy is associated with the high frequency eddies.

Following Sheng and Hayashi (1989a, b) the energy cycles are summarized in Fig. 4 by regrouping the spectra into motions of the time-mean, low frequency, which represents approximately the period range between the synoptic time scales and about 90 days, and high frequency, which represents the synoptic time scales shorter than 10 days. Fig. 4c was also shown in Sheng and Hayashi (1989b). Each box in the figures represents an energy reservoir of labeled form and frequency range, containing the amount of energy shown in the bottom of the box in units of 10^4 J/m^2 . The arrows indicate the directions of energy flow, and the values under give the magnitudes of energy transfer in units of W/m^2 . The three energy cycles depicted are very similar and they have been confirmed by the FGGE year data analysed at ECMWF and GFDL (Sheng and Hayashi, 1989a). The general picture revealed by the calculation is one of available potential energy being generated by diabatic heating largely at the time-mean scale and flowing to transient disturbances of both high and low frequencies through the eddy heat transfer processes measured by LA. A smaller amount of APE is also transferred down to shorter

time scales by the nonlinear exchanges, NA. At the same time, potential energy is converted into kinetic energy at all frequency groups. It is noted that significantly more energy is converted at the fast transient group than the slow transient group, and therefore, it is a signature that baroclinic instability dominates the high frequency disturbances. By nonlinear exchanges measured by NK, kinetic energy is then transferred into longer time scales. A salient feature that distinguishes the energy balance of the slow transients from that of the fast transients is that baroclinic conversion, although still important, is no longer the unique energy source for the transient KE. Important contributions also come from both AK and NK, and to some extent, from LK, as will be evident in discussions of local energy contributions in the next two sections.

The seasonal contrast of energy cycles can be summarized simply by noting that we observe higher energy levels and energy conversions in the wintertime than in the summertime while the general directions of energy flow are kept unchanged, with a few exceptions that we now discuss. Firstly the baroclinic conversion for the time-mean flow is weaker in the winter season. A closer inspection reveals that the hemispheric mean value of this term is a result of a close competition between the positive contribution from the lower latitudes where the Hadley cells prevail, and the negative contribution from the extratropics. In the summertime as the Hadley cell in the Southern Hemisphere marches northward slightly across the equator, the positive contribution from the tropics increases significantly.

Another exception is the seasonal reversal of barotropic conversion LK in the low frequency range. Consistent with the results of Wallace and Lau (1985), the LK term in the cold season is positive, indicating an energy

supply to the slow transients (Fig. 4a). The magnitude of the conversion, however, is small and it takes the mean flow about 33 days to replenish the KE reservoir. An estimate of 14 days was reached by Wallace and Lau based upon 300 mb data only. On the other hand, AK and NK are calculated to give amplification times of 10 and 11 days, respectively. It is of interest that during the summertime the seasonal mean flow extracts KE from the slow transients and appears to be barotropically stable (Fig. 4b). According to the detailed analysis of Wallace and Lau, it is the zonal asymmetry of the wintertime stationary waves that overcomes the contribution from the convergence of meridional momentum flux into the jet stream and provides the net supply of KE to the slow transients. In view of the present results, the strength of the summertime stationary waves do not appear strong enough for the convergence of zonal momentum flux to be dominant in LK, and the same can be stated for the annual mean case (Fig. 4c).

4. Local contributions to the wintertime energetics

Our main interest in this section is the local contributions of spectral energetics to the maintenance of transient eddies with short or long periods. In the presentation that follows a contrast is drawn between the fast and the slow transients. All the variables shown have been vertically integrated and the units are in J/m^2 for energy and W/m^2 for conversion terms. Since the circulation statistics involve either high order moments or high order derivatives, the results have been spectrally filtered by retaining spherical harmonics triangularly truncated at zonal wavenumber 12. The

weakly filtered data contain at least 85 per cent of their original variance.

Fig. 5 shows the distribution of the kinetic energy during the Northern Hemisphere winter for the transients with periods shorter than 10 days. It is characterized by elongated maxima over the western Atlantic around 40°N and the central Pacific at slightly lower latitude. The zone of maximum in the Atlantic is oriented somewhat in the northeast-southwest direction. These two regions can be identified as storm tracks, which can also be shown by the high frequency variance of transient geopotential heights as in Blackmon et al. (1977). Storm tracks occur downstream and slightly poleward of the 200mb jet stream where baroclinicity is most intense. A third region of high variance, though much weaker, can be located east of the Urals. The Tibetan Plateau and the Rockies, which separate the Atlantic and the Pacific maxima, are noted to have low values of KE. These features are consistent with the results documented in Blackmon et al. (1977), in which 2.5 - 6 day high-pass filtered geopotential height at 500mb was used to characterize the fast transients. One notable difference is that the centre near the Urals was much stronger in Blackmon et al's geopotential analyses.

The distribution of available potential energy for the fast transients is shown in Fig. 6. The high frequency maxima are located over the western Atlantic and Pacific regions, somewhat westward of the fast transient KE. The third maximum east of the Urals is, however, less visible in the APE map. The similarity among the patterns of KE, APE and the baroclinic conversion term, AK (Fig. 7), in the high frequency range is remarkable. These features of the high frequency energetics are consistent with the classical theory of baroclinic instability, modified by local intensifications of dis-

turbances due to land-ocean contrasts and orographic forcing. The wintertime stationary waves tend to organize baroclinic eddies in elongated storm tracks without dramatically changing their essential wave structure, evolution and energetics. Frederiksen (1979a, b, 1983) was able to simulate, in a linear baroclinic stability analysis of the longitudinally dependent climatological mean flow, the observation that the fastest growing baroclinic wave modes exhibit their largest amplitudes in the storm track regions. Hoskins (1983) also discussed the role of time-mean flow in maintaining the storm track structure.

The barotropic transfer of KE from the time-mean flow into the fast transients, LK, also indicates well defined patterns (Fig. 8). The synoptic scale eddies lose KE mainly in two regions, the western Atlantic and eastern Pacific. In the Atlantic region, the maximum energy loss is located slightly east of the maximum centre of KE, while its Pacific counterpart is near 160°W and 30°N . The positive conversion is found over the North American continent. The entire Eurasia and west Pacific show signs of weak but positive values. The patterns are very similar to those of Wallace and Lau (1985), except that the present centre in the Pacific is about 20 degrees further east.

The modeling study by Simmons and Hoskins (1978) on the time evolution of nonlinear transient disturbances illustrates the life cycle of synoptic eddies. Baroclinic waves superimposed on a balanced zonal mean flow are seen to grow initially by baroclinic instability with vigorous generations of eddy APE and KE. After about one week of model simulation, these disturbances reach the occluded stage and become more nearly barotropic with a correspondingly much weakened heat flux. As the waves propagate further east-

ward, the structure of the momentum fluxes generally results in the transfer of KE from the transient eddies into the mean flow. In the atmosphere, eastern Asia and eastern North America are observed to have strong vertical wind shears and therefore are propitious sites for the initiation of baroclinic development of synoptic scale cyclones. As the disturbances move along the storm tracks they gradually acquire a barotropic structure. In terms of energetics of the high frequency transients discussed in this section, the theoretical and modeling results seem capable of providing a sound framework to explain the geographic distributions of the energy conversion terms.

Fig. 9 shows the distribution of kinetic energy during the wintertime for the transients with periods longer than 10 days. The most salient features are the two maxima, less elongated in the east-west direction than for the fast transients (Fig. 5), located to the east of the high frequency maxima and at somewhat higher latitudes (about 5 degrees). In comparison with the maxima of low frequency variance derived from the 500mb height field, these centres of transient activities are located further eastward and at slightly lower latitudes (see Blackmon et al., 1977). It is noted also that the third maximum over the Siberian arctic, usually appearing in the variance of the 500mb geopotential height, is hardly traceable in our KE analysis. These preferred locations of low frequency activities appear to be related to regions of frequent blocking, identified by Rex (1950) and documented more recently by Dole (1986). The regions of minimum slow transient activity, as in the case of the fast transients, are found over the Tibetan Plateau and the Rockies.

The geographical distribution of the low frequency APE (Fig. 10) is fundamentally different from that of KE. The two major maxima are located

over North America and eastern Mongolia. No strong centres can be found in either the Atlantic or the Pacific region. Unlike their high frequency counterparts, wind disturbances of slow transients are associated with no significant temperature perturbations, which is another way of saying that the low frequency eddies have a barotropic or quasi-barotropic structure, as found by Blackmon et al. (1979). The latter showed that in the eastern oceans the low frequency fluctuations of geopotential height exhibit a barotropic structure, whereas the continental regions to the north and east of the Rockies and Himalayas are notable for their more baroclinic structure. Our results are consistent with theirs.

The geographical distribution of the integrand appearing in AK , the baroclinic energy conversion, is shown in Fig. 11 for the low frequency disturbances. The main maxima are located over North America and the northern Pacific ocean. It is of interest that AK is either negative or weakly positive over the eastern oceans, where the kinetic energy of the slow transients is strongest. The results presented in Sheng and Hayashi (1989a, b) and in Section 3 of this paper all indicate that, for area-integrated quantities, the baroclinic conversion is the major energy source for the low frequency eddies, not only in the wintertime but also in the annual mean sense. It is interesting to note that the main contributions to the integrand appearing in AK^b does not come from the eastern oceanic regions.

The barotropic KE conversion from the slow transients to the time-mean flow, BT^b (see Appendix A) is shown in Fig. 12. The most significant features are two negative centres in the mid-oceans where the time-mean flow loses kinetic energy to the transient eddies. It is noted that the regions of strong KE conversion are located downstream of the jet-stream exit, sug-

gesting that, as proposed by Hoskins et al. (1983), the low frequency transients, elongated in the east-west direction, produce a westward \vec{E} vector (Wallace and Lau, 1985), implying a down-gradient flux of momentum and a transfer of KE from the mean flow to the slow transients. Comparing Fig. 12 with Fig. 8, it is evident that the mean flow supplies KE to the slow transients near where it extracts KE from the fast transients, by the mechanism of a up-gradient flux of momentum (not shown).

It is stressed that due to the existence of a mean flow transport of transient KE, the local energy gain by the transients LK does not equal the local energy loss by the mean flow shown in Fig. 12 (cf. Appendix A). The barotropic KE conversion term LK^b is illustrated in Fig. 13, which sharply contrasts the picture displayed in Fig. 12. Positive centres are located over the west coasts of North America and Europe, extending towards the southwest direction. Negative values of LK^b are found in the western parts of the Atlantic and Pacific, where the low frequency KE is relatively weak. By comparison with the baroclinic conversion AK^b , the barotropic term apparently shows a better correspondence with the kinetic energy in terms of the geographic distributions.

The gain of kinetic energy by the slow transients due to the nonlinear interactions with the fast transient eddies, NK^b , is shown in Fig. 14. It is very interesting to see some similarities between the patterns shown in Figs. 13 and 14. Once again positive regions are present in the eastern parts of Atlantic and Pacific. Due to the smaller negative contributions from the west oceans, the net conversion from NK^b is much greater than LK^b when averaged over the entire Northern Hemisphere, as was discussed in Section 3.

Frederiksen (1983b) conducted a linear stability analysis of a three-dimensional model with a realistic wintertime mean state. A variety of unstable modes were obtained, including propagating cyclogenesis modes, onset-of-blocking modes and low frequency "teleconnection" modes. It was found that, for an increasingly larger static stability parameter, the fastest growing modes in the model assume a structure that is more and more barotropic. Nevertheless, the baroclinic energy conversion did enhance the growth rate of the unstable modes even with very low frequencies. In our hemispherically averaged energetics, we find that in winter the main sources of low frequency KE (Fig. 4a) are the baroclinic conversion and the transfer of KE from the fast transients. While smaller by a factor of about 3, the transfer of KE from the time mean flow to the slow transients is still of some importance. The lack of contribution from the baroclinic energy conversion in the regions of strong low frequency KE is in agreement with the quasi-barotropic structure found by Blackmon et al. (1979).

Our current understanding of the relationship between the low frequency variability and the theory of barotropic instability is based to a large extent upon the studies by Simmons et al. (1983) and Wallace and Lau (1985), who have provided ample evidence of the barotropic extraction of kinetic energy by the slow transients from the wintertime climatological mean flow. More recently Nakamura et al. (1987) demonstrated that five typical teleconnection patterns are all associated with an energy conversion in the sense described above. The Pacific/North American and Eastern Atlantic patterns were found to have by far the largest conversions, due to the fact that these patterns have "seesaws" located in the jet-exit regions and therefore obtain KE more effectively than the other patterns. The evidence presented

in Figs. 12 and 13 indicates that KE is extracted from the jet-exit regions and supplied to the low frequency transients further downstream. Therefore the notion of barotropic energy conversion from the time-mean flow into the eddies and the barotropic instability due to the zonal and meridional variations of mean flow are still valid even in a baroclinic basic state.

The transfer of KE into the low frequency transients from the high frequency baroclinic waves (Fig. 14) exhibits a horizontal distribution which is similar to the barotropic term (Fig. 13). This suggests that the slow transients are organized by the wintertime stationary waves in such a way to extract KE from not only the mean flow but also from the synoptic scale eddies in the eastern parts of the major oceans. The barotropic instability and the forcing by the high frequency transients function coherently to enhance the low frequency transients. It would seem that the low frequency regime, in some sense, should be considered as a barotropically unstable system forced by the fast transients, instead of a barotropically free unstable system. This is consistent with the results of Mullen (1987), Holopainen and Fortelius (1987), and Lau (1988) who examined the relationship between the slowly varying part of the flow and the fast baroclinic waves; they found that the latter tend to reinforce the time fluctuations present in the former. According to the calculations shown in Section 3 and the present Section, nonlinear interactions provide much more KE to the wintertime slow transients than the barotropic processes do and, therefore, are of importance both locally and hemispherically for the energy balance of the low frequency regime. At this stage little is known about the structure and evolution of the low frequency momentum and thermal forcings due to the nonlinear interactions with the high frequency eddies. Shutts (1983) did, how-

ever, conduct numerical simulations of eddy forcing during an Atlantic blocking episode, which provided a basis for a qualitative understanding of the process.

5. Local contributions to the summertime energetics

It was demonstrated in Section 3 that the energy cycle experiences strong seasonal oscillations in all the frequency bands discussed, with the APE and KE levels showing consistently higher values in the winter season. The energy conversion terms undergo more complicated evolutions, and a significant example is the reversal of the barotropic conversion of KE for the low frequency transients. In this section, the energetics of the summer season are further studied in terms of local contributions to the hemispheric integrals.

The distributions of kinetic energy is shown in Fig. 15 for the high frequency transients. A comparison with Fig. 5 reveals that the geographic patterns of KE are similar for the winter and the summer seasons. The storm tracks are still located in the Atlantic and Pacific oceans, but at somewhat higher latitudes, in agreement with the modelling results of Frederiksen (1983a). The strength of the storm activities is considerably reduced, especially in the Atlantic region. It is also noted that the storm tracks are less elongated in the zonal direction when compared with their counterparts in the winter season. Other features, such as the third maximum east of the Urals and the relatively low values near the Rockies and the Tibetan Plateau, are still traceable but less significant. Shown in Fig. 16 is the distribution of available potential energy for the fast transients. The elong-

ated maxima are clearly related to the storm tracks, but shifted westward. These are indications that high frequency transients are baroclinic disturbances, as in the winter season. Fig. 17 shows the patterns of baroclinic conversion, AK^b , which share a clear resemblance with those of KE and APE. In view of the present results, we conclude that the high frequency eddies still owe their origin to the baroclinic instability of the three dimensional flow, although the baroclinicity of the summertime mean state is much weaker than that of the wintertime.

It comes as no surprise that the local energy balance of the fast transients in summer is very similar to that in winter, as can be expected from the similarity of the hemispherically integrated energy cycles for the summer and winter seasons. We find, however, that similarities also exist in the energy balance of the slow transients, even though the role of the barotropic energy conversion is reversed for the two seasons.

Fig. 18 shows the geographical distribution of kinetic energy for the slow transients. The centres of maximum activity are located significantly eastward of the positions of the summertime storm tracks. The energy level of maximum KE is diminished considerably in comparison with the wintertime. Fig. 19 shows the same as Fig. 18 but for the available potential energy. Two maxima can be found in the continental regions of northern Canada and west Siberia, which are completely out of phase with the active regions of low frequency wind variability. By the same argument as that presented in Section 4, the lack of association between KE and APE is consistent with the quasi-barotropic structure of the low frequency transients as discussed in Blackmon et al. (1977).

The local baroclinic energy conversion AK is shown in Fig. 20 for the

slow transients. The major contributions are from Canada and, from east China extending to the western Pacific. No significant baroclinic conversion is found in the regions of strong low frequency KE, as was also observed for the winter case. It is evident that the baroclinic energy conversion is hindered by the quasi-barotropic structure of the slow transients. LK^b , the barotropic conversion of KE, is presented in Fig. 21. In much the same way as in the winter season, the stationary waves serve to supply KE and organize the transient activities in the eastern parts of the Atlantic and Pacific oceans. However, the western parts of the oceans are occupied by negative conversions, which results in a net transfer of KE from the eddies to the mean flow in a hemispheric integration (Fig. 4b). Again, the dipole appearance of the patterns in Fig. 21 suggests that the advective part of the expression for LK^b is locally dominant, which does not contribute to the hemispheric average. The negative value obtained for the hemispherically averaged LK^b (Fig. 4b) indicates that the summer time stationary waves are not sufficiently strong to support the mechanism of barotropic instability proposed by Simmons et al. (1983). Fig. 22 shows the contribution from the sum of LK^b and NK^b , which shares many features of LK^b . It is therefore suggestive that, in a sense, the interactions with the synoptic scale eddies act as a forcing upon a barotropically stable mean state, which arranges the sites for the activities of the slow transients.

6. Conclusions

In the present study, spectral energetics in the frequency domain have been calculated using the ECMWF operational analyses for the winter and summer seasons separately and the following conclusions are of interest:

(i) The atmospheric energetics in the frequency domain undergo a seasonal cycle such that the annual variation is stronger in the high frequency band than in the low frequency band. Generally the levels of energy and energy conversion terms are both higher in the wintertime, as would be expected. When integrated over the Northern Hemisphere, the baroclinic conversion is the primary KE source for both winter and summer seasons for the three frequency groups considered. For the low frequency transients, the nonlinear exchanges of kinetic energy, i.e., the energy supplied by the synoptic scale disturbances, are also important. The barotropic conversion of kinetic energy (between the time-mean flow and the low frequency transients) changes sign from the cold to the warm season; the climatological mean flow appears to be barotropically unstable in winter but stable in summer.

(ii) The geographical distributions of KE and APE for different frequency bands indicate that high frequency disturbances are organized by the time-mean flow and that the low frequency ones are most active further east where the phenomenon of blocking frequently occurs. One of the important observations is that the slow transients are of a quasi-barotropic structure, which is indicated by the separation of the KE and APE centres.

(iii) In both winter and summer seasons, the distributions of energy and energy conversion terms for the synoptic scale eddies are in good agreement with the classical theory of baroclinic instability modified by the

presence of stationary waves. The fast transients are observed to be baroclinically unstable and barotropically stable.

(iv) The baroclinic conversion for the slow transients is weak in the eastern parts of the Atlantic and Pacific oceans where the level of low frequency KE is high. Although the domain-integrated value of the barotropic conversion is negative in the summertime, its spatial distribution is in many ways similar to that in the wintertime. It is very interesting that the nonlinear and barotropic conversions of KE seem to reinforce each other and enhance the low frequency activities in the eastern parts of the major oceans. Our results suggested that, in the wintertime, the low frequency disturbances can be viewed as modes that are forced by the fast baroclinic eddies and growing in a barotropically unstable, zonally varying basic state.

The spectral energetics studied in Sheng and Hayashi (1989a, b), with data sets from observations during the FGGE year and simulations at GFDL, demonstrated that kinetic energy of the low frequency transients is primarily maintained by the conversion from the available potential energy. Schubert (1986) found that the net barotropic and baroclinic conversions were of comparable magnitudes for periods greater than 10 days while the baroclinic conversion dominates for shorter period. The observational study of Wallace and Lau (1985), using observational and GCM data sets, confirmed that the barotropic energy conversion is an important energy source for the slow transients in the wintertime. Nakamura et al. (1989) have also shown that the major teleconnection patterns are structured to extract KE from the zonally varying climatological mean flow. From the results presented above,

the energy balance of the slow transients seems more complicated than it was previously thought to be. Although the baroclinic conversion is the major energy source for the Northern Hemisphere as a whole, the barotropic and the nonlinear conversions provide the main features of the local energy balance over the eastern Atlantic and Pacific. Moreover, the nonlinear effects are even more important in the summer season since, in a hemispherically averaged sense, the mechanism of barotropic instability supplies no net energy to the disturbances.

The limitations of the ECMWF data set has to be properly addressed. It is well known that ECMWF analyses systematically underestimate the divergence component of the wind field, mainly in the tropics. The energy cycles during the FGGE year computed from the ECMWF and GFDL data sets show considerable discrepancy in spectral estimates of baroclinic energy conversion, although the general agreement was found on directions and magnitudes of the energy flow (Sheng and Hayashi, 1989a). Therefore, the geographic distributions of the baroclinic energy conversion is subject to some uncertainty and caution has to be exercised in their interpretations. However, since we have only shown maps of the extratropical region (north of 20°N), this problem may not seriously affect our main conclusions.

Finally, it should be realized that the results presented in the present study apply to the average behaviour of the atmosphere over the period considered. It is quite conceivable that during subperiods the behaviour may be quite different. For example, energy transfers taking place during the life cycle of an atmospheric blocking, as in the case studied by Holopainen and Fortelius (1987), need not be the same as those presented here. Nevertheless, it is of interest to document the average features of the atmos-

phere. In addition to being of interest by themselves, the results may be quite useful in evaluating the performance of general circulation models.

Appendix A

Spectral energy equations for KE and APE

The derivations of the spectral energy equations in the frequency domain were presented in Sheng (1986) and Sheng and Hayashi (1989a). The equations of KE and APE for the low and high frequency bands can be written as,

$$LK^{\ell} + NK^{\ell} + AK^{\ell} + FK^{\ell} + FP^{\ell} - D^{\ell} = 0,$$

$$LK^h + NK^h + AK^h + FK^h + FP^h - D^h = 0,$$

$$LA^{\ell} + NA^{\ell} - AK^{\ell} + FA^{\ell} + G^{\ell} = 0,$$

$$LA^h + NA^h - AK^h + FA^h + G^h = 0.$$

Here the superscripts ℓ and h denote the energy transfer terms for the low and high frequency bands, respectively. The mathematical expression for each term is given as the following:

$$LK^{\ell} = - \frac{u_{\ell} [\nabla \cdot (\bar{u}\bar{v}_{\ell} + u_{\ell}\bar{v}) - \frac{\tan\phi}{a} (\bar{u}v_{\ell} + u_{\ell}\bar{v})]}{v_{\ell} [\nabla \cdot (\bar{v}\bar{v}_{\ell} + v_{\ell}\bar{v}) + \frac{\tan\phi}{a} (\bar{u}u_{\ell} + u_{\ell}\bar{u})]},$$

$$LK^h = - \frac{u_h [\nabla \cdot (\bar{u}\bar{v}_h + u_h\bar{v}) - \frac{\tan\phi}{a} (\bar{u}v_h + u_h\bar{v})]}{v_h [\nabla \cdot (\bar{v}\bar{v}_h + v_h\bar{v}) + \frac{\tan\phi}{a} (\bar{u}u_h + u_h\bar{u})]},$$

$$NK^{\ell} = - \frac{u_{\ell} [\nabla \cdot (u_{\ell}v_h + u_hv_{\ell} + u_hv_h) - \frac{\tan\phi}{a} (u_{\ell}v_h + u_hv_{\ell} + u_hv_h)]_{\ell}}{v_{\ell} [\nabla \cdot (v_{\ell}v_h + v_hv_{\ell} + v_hv_h) + \frac{\tan\phi}{a} (u_{\ell}u_h + u_hu_{\ell} + u_hu_h)]_{\ell}},$$

$$NK^h = - \frac{u_h [\nabla \cdot (u_{\ell}v_h + u_hv_{\ell} + u_{\ell}v_{\ell}) - \frac{\tan\phi}{a} (u_{\ell}v_h + u_hv_{\ell} + u_{\ell}v_{\ell})]_h}{v_h [\nabla \cdot (v_{\ell}v_h + v_hv_{\ell} + v_{\ell}v_{\ell}) + \frac{\tan\phi}{a} (u_{\ell}u_h + u_hu_{\ell} + u_{\ell}u_{\ell})]_h},$$

$$FK^t = - \nabla \cdot \overline{\left[\frac{1}{2}(u_t^2 + v_t^2)v_t \right]},$$

$$FK^h = - \nabla \cdot \overline{\left[\frac{1}{2}(u_h^2 + v_h^2)v_h \right]},$$

$$FP^t = - \nabla \cdot \overline{(\phi_t v_t)},$$

$$FP^h = - \nabla \cdot \overline{(\phi_h v_h)},$$

$$D^t = - \overline{(u_t F_t + v_t F_t)}$$

$$D^h = - \overline{(u_h F_h + v_h F_h)}$$

$$AK^t = - \overline{\omega_t \alpha_t},$$

$$AK^h = - \overline{\omega_h \alpha_h},$$

$$LA^t = - \gamma \overline{\theta_t^* \nabla \cdot (\theta_t^* \overline{v} + \overline{\theta^*} v_t)},$$

$$LA^h = - \gamma \overline{\theta_h^* \nabla \cdot (\theta_h^* \overline{v} + \overline{\theta^*} v_h)},$$

$$NA^t = - \gamma \overline{\theta_t^* \nabla \cdot (\theta_t^* v_h + \theta_h^* v_t + \theta_h^* v_h)_t},$$

$$NA^h = - \gamma \overline{\theta_h^* \nabla \cdot (\theta_t^* v_h + \theta_h^* v_t + \theta_t^* v_t)_h},$$

$$FA^t = - \gamma \nabla \cdot \overline{\left(\frac{1}{2} \theta_t^{*2} v_t \right)},$$

$$FA^h = -\gamma \nabla \cdot \left(\frac{1}{2} \overline{\theta_h^{*2} v_h} \right),$$

$$G^l = \gamma \left(\frac{\theta}{C_p T} \right) \overline{\theta_l^* Q_l^*},$$

$$G^h = \gamma \left(\frac{\theta}{C_p T} \right) \overline{\theta_h^* Q_h^*}.$$

In the above equations, all time series have been decomposed into the time-mean, the low frequency and the high frequency parts,

$$f = \bar{f} + f_l + f_h.$$

A list of symbols, definitions and variables are given in Appendix B. The expression for the barotropic conversion, LK, represents the kinetic energy locally transferred into the transient eddies. Figs. 8 and 13 illustrate the geographical distribution of this term for the high and the low frequency bands, respectively. On the other hand, an alternative equation for the barotropic conversion can be derived by mass averaging LK over a closed domain and performing an integration by parts,

$$\begin{aligned} (BT^l) &= - (LK^l) \\ &= \overline{u_l v_l \cdot \nabla u} + \overline{v_l v_l \cdot \nabla v} + \frac{\tan \phi}{a} [\overline{u_l v_l u} - \overline{u_l u_l v}]. \end{aligned}$$

$$\begin{aligned} (BT^h) &= - (LK^h) \\ &= \overline{u_h v_h \cdot \nabla u} + \overline{v_h v_h \cdot \nabla v} + \frac{\tan \phi}{a} [\overline{u_h v_h u} - \overline{u_h u_h v}]. \end{aligned}$$

Here $\{f\}$ represents the mass average of a function f . The integrand of the

above expression for BT is shown in Fig. 12 for the low frequency band. It is seen that, when integrated over a closed domain, LK is identical to BT but with the opposite sign. The local difference between the two expressions is due to the transport of transient KE by the time-mean flow (Hayashi, 1980), which vanishes upon integration over the mass of the atmosphere. Wallace and Lau (1985) essentially applied the formula for BT, with some simplifications, to their single level data sets to calculate the barotropic KE conversion.

Appendix B

a	earth's radius
C_p	specific heat at constant pressure.
F_u	friction force in the x-direction
F_v	friction force in the y-direction
g	force of gravity per unit mass
p	pressure
Q	diabatic heating
T	temperature
u	eastward component of velocity
v	northward component of velocity
V	three-dimensional velocity vector
z	geopotential height
α	specific volume
γ	static stability parameter
θ	potential temperature
ϕ	latitude
ω	vertical pressure velocity
$\overline{(\)}$	time average
$\{(\)\}$	mass average
$(\)^*$	deviation from the horizontal mean
$(\)_h$	high frequency component of a time series
$(\)^h$	energy transfer term for the high frequency band
$(\)_l$	low frequency component of a time series

() ⁶	energy transfer term for the low frequency band
∇	three-dimensional gradient operator
AK	baroclinic conversion from APE to KE
D	dissipation of transient KE
FA	convergence of transient APE flux
FK	convergence of transient KE flux
FP	convergence of transient flux of potential energy
G	generation of transient APE
LA	transfer of APE from the time-mean flow into the transient eddies
LK	transfer of KE from the time-mean flow into the transient eddies
NA	transfer of APE due to nonlinear interactions of transient eddies
NK	transfer of KE due to nonlinear interactions of transient eddies
BT	an alternative expression for barotropic energy conversion

REFERENCES

- Blackmon, M.L., Wallace, J.M., Lau, N.-C. and Mullen, S.L. 1977. An observational study of the Northern Hemisphere wintertime circulation. *J. Atmos. Sci.* 34, 1040-1053.
- Blackmon, M.L., Madden, R.A., Wallace, J.M. and Gutzler, D.S. 1979. Geographical variations in the vertical structure of geopotential height fluctuations. *J. Atmos. Sci.* 36, 2450-2466.
- Charney, J.G. 1947. The dynamics of longwaves in a baroclinic westerly current. *J. Meteor.* 4, 135-163.
- Chen, T.C. and Wiin-Nielsen, A. 1978. On nonlinear cascades of atmospheric energy and enstrophy in a two dimensional spectral index. *Tellus.* 30, 313-322.
- Dole, R.M. 1986. Persistent anomalies of the extratropical Northern Hemisphere wintertime circulation: Structure. *Mon. Wea. Rev.* 114, 178-207.
- Eady, E.T. 1949. long waves and cyclone waves. *Tellus.* 1, 33-52.
- Frederiksen, J.S. 1979a. The effect of long planetary waves on the regions of cyclogenesis: linear theory. *J. Atmos. Sci.* 36, 195-204.
- Frederiksen, J.S. 1979b. Baroclinic instability of zonal flows and planetary waves in multi-level models on a sphere. *J. Atmos. Sci.* 36, 2320-2335.
- Frederiksen, J.S. 1983a. Disturbances and eddy fluxes in Northern Hemisphere flows: Instability of three-dimensional January and July flows. *J. Atmos. Sci.* 40, 836-855.
- Frederiksen, J.S. 1983b. A unified three-dimensional instability theory of the onset of blocking and cyclogenesis. II: Teleconnection patterns. *J. Atmos. Sci.*, 40, 2593-2609.

- Hayashi, Y. 1980: Estimation of nonlinear energy transfer spectra by the cross-spectral method. *J. Atmos. Sci.* 37, 299-307.
- Holopainen, E. and Fortelius, C. 1987. High frequency eddies and blocking. *J. Atmos. Sci.* 44, 1632-1645.
- Hoskins, B.J. 1983: Modelling of the transient eddies and their feedback on the mean flow. In "large-Scale Dynamical Processes in the Atmosphere" (Hoskins, B.J. and Pearce, R.P., eds.), Academic Press, New York, 169-199.
- Hoskins, B.J. James, I.N. and White, G.H. 1983. The shape, propagation and mean-flow interaction of large scale weather systems. *J. Atmos. Sci.* 40, 1595-1612.
- Kuo, H.-L. 1949. Dynamical instability of two dimensional nondivergent flow in a barotropic atmosphere. *J. Meteor.* 6, 105-122.
- Lau, N.-C. 1988. Variability of the observed midlatitude cyclone tracks in relation to low-frequency changes in the circulation pattern. *J. Atmos. Sci.* 45, 2718-2743.
- Lorenz, E.N. 1967. The Nature and Theory of the General Circulation of the atmosphere. World Meteorological Organisation, Geneva, Switzerland, 161 pp.
- Mullen, S.L. 1987. Transient eddy forcing of blocking flows. *J. Atmos. Sci.* 44, 3-22.
- Nakamura, H. Tanaka, M. and Wallace, J.M. 1987. Horizontal structure and energetics of Northern Hemisphere wintertime teleconnection patterns. *J. Atmos. Sci.* 44, 3377-3391.
- Rex, D.F. 1950. Blocking action in the middle troposphere and its effect upon regional climate. II. The climatology of blocking action. *Tellus.*

- 2, 275-301.
- Saltzman, B. 1970. Large-scale atmospheric energetics in the wave number domain. *Rev. Geophys. Space. Phys.* 8, 289-302.
- Schubert, S.D. 1986. The structure, energetics and evolution of the dominant frequency-dependent three dimensional atmospheric modes. *J. Atmos. Sci.* 43, 1210-1237.
- Sheng, J. 1986. On the energetics of low frequency motions. Ph. D. dissertation. Department of Meteorology, Florida State University, Tallahassee, Florida. 186 pp.
- Sheng, J. and Hayashi, Y. 1989a. Estimation of atmospheric energetics in the frequency domain during the FGGE year. *J. Atmos. Sci.* in press.
- Sheng, J. and Hayashi, Y. 1989b. Observed and simulated energy cycles in the frequency domain. *J. Atmos. Sci.* in press.
- Shutts, G.J., 1986. A case study of eddy forcing during an Atlantic blocking episode. *Adv. in Geophys.* 29, 135-164.
- Simmons, A.J. and Hoskins, B.J. 1978: The life cycles of some nonlinear baroclinic waves. *J. Atmos. Sci.* 35, 414-432.
- Simmons, A.J. Wallace, J.M. and Branstator, G.W. 1983. Barotropic wave propagation and instability, and atmospheric teleconnection patterns. *J. Atmos. Sci.* 40, 1363-1392.
- Wallace, J.M. and Lau N.-C. 1985. On the role of Barotropic energy conversion in the general circulation. *Adv. Geophys.* 28A, 33-74.

Figure Legends

- Fig. 1 Spectral distributions of KE, plotted with a constant interval of log-frequency. In units of J/m^2 . The leftmost bar indicates the value for the time-mean. For (a) winter, (b) summer and (c), annual mean.
- Fig. 2 As in Fig. 1, but for APE.
- Fig. 3 As in Fig. 1, but for baroclinic conversion term. In units of W/m^2 .
- Fig. 4 Schematic depiction of the atmospheric energy cycle in the frequency domain. Numbers in boxes denote the energy storage in units of $10^4 \text{ J}/\text{m}^2$, and fluxes of energy in W/m^2 . For (a) winter, (b) summer and (c) annual mean.
- Fig. 5 Winter ECMWF high frequency KE. Vertically integrated with contour interval $10^5 \text{ J}/\text{m}^2$.
- Fig. 6 Winter ECMWF high frequency APE. Vertically integrated with contour interval $10^5 \text{ J}/\text{m}^2$.
- Fig. 7 Winter ECMWF high frequency AK. Vertically integrated with contour interval $1.0 \text{ W}/\text{m}^2$.

- Fig. 8 Winter ECMWF high frequency LK. Vertically integrated with contour interval 1.0 W/m^2 .
- Fig. 9 Winter ECMWF low frequency KE. Vertically integrated with contour interval 10^5 J/m^2 .
- Fig. 10 Winter ECMWF low frequency APE. Vertically integrated with contour interval 10^5 J/m^2 .
- Fig. 11 Winter ECMWF low frequency AK. Vertically integrated with contour interval 0.5 W/m^2 .
- Fig. 12 Winter ECMWF low frequency BT. Vertically integrated with contour interval 0.5 W/m^2 .
- Fig. 13 Winter ECMWF low frequency LK. Vertically integrated with contour interval 1.0 W/m^2 .
- Fig. 14 Winter ECMWF low frequency NK. Vertically integrated with contour interval 1.0 W/m^2 .
- Fig. 15 Summer ECMWF high frequency KE. Vertically integrated with contour interval 10^5 J/m^2 .
- Fig. 16 Summer ECMWF high frequency APE. Vertically integrated with

contour interval 10^5 J/m^2 .

Fig. 17 Summer ECMWF high frequency AK. Vertically integrated with contour interval 0.5 W/m^2 .

Fig. 18 Summer ECMWF low frequency KE. Vertically integrated with contour interval 10^5 J/m^2 .

Fig. 19 Summer ECMWF low frequency APE. Vertically integrated with contour interval 10^5 J/m^2 .

Fig. 20 Summer ECMWF low frequency AK. Vertically integrated with contour interval 0.5 W/m^2 .

Fig. 21 Summer ECMWF low frequency LK. Vertically integrated with contour interval 0.5 W/m^2 .

Fig. 22 Summer ECMWF low frequency LK + NK. Vertically integrated with contour interval 0.5 W/m^2 .

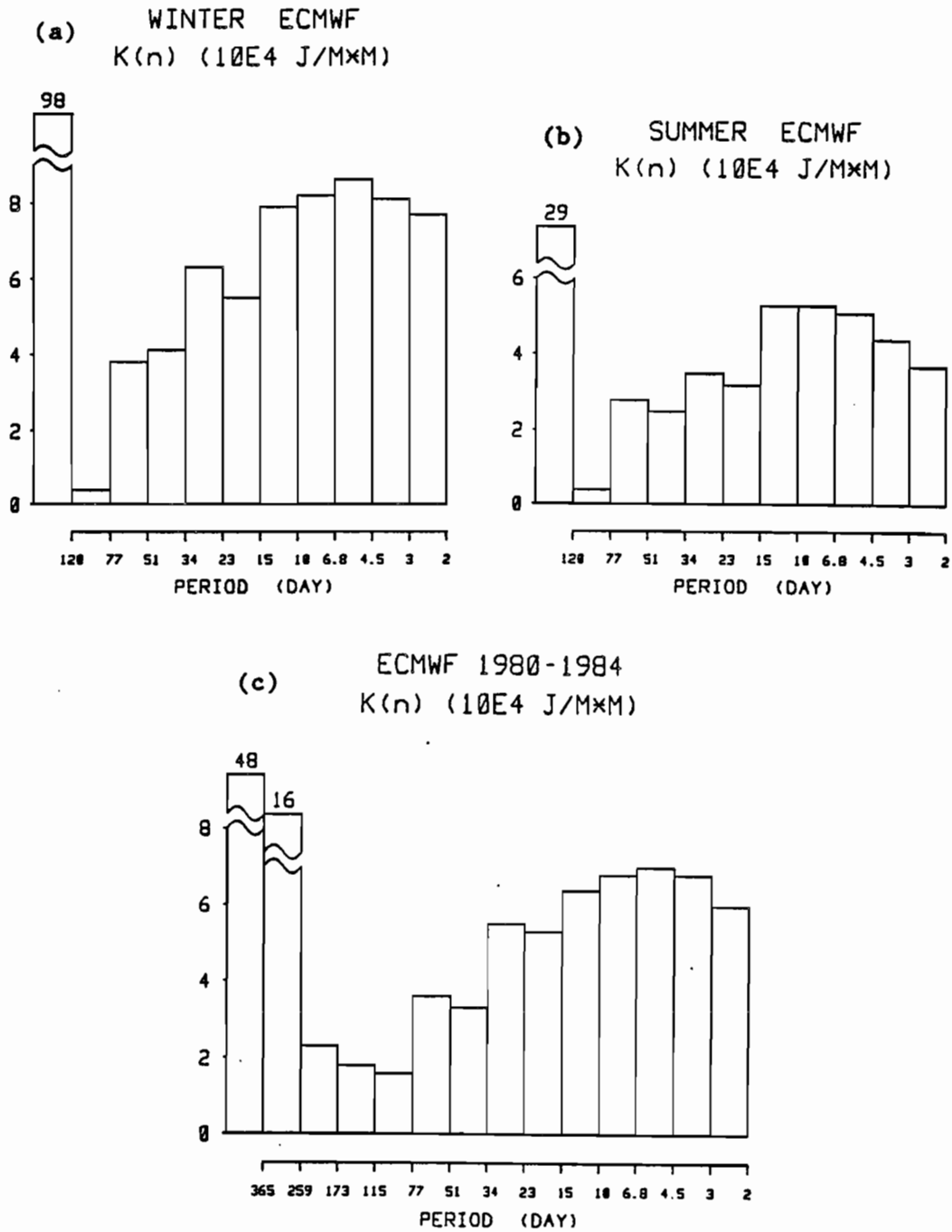


Fig. 1 Spectral distributions of KE, plotted with a constant interval of log-frequency. In units of J/m^2 . The leftmost bar indicates the value for the time-mean. For (a) winter, (b) summer and (c), annual mean.

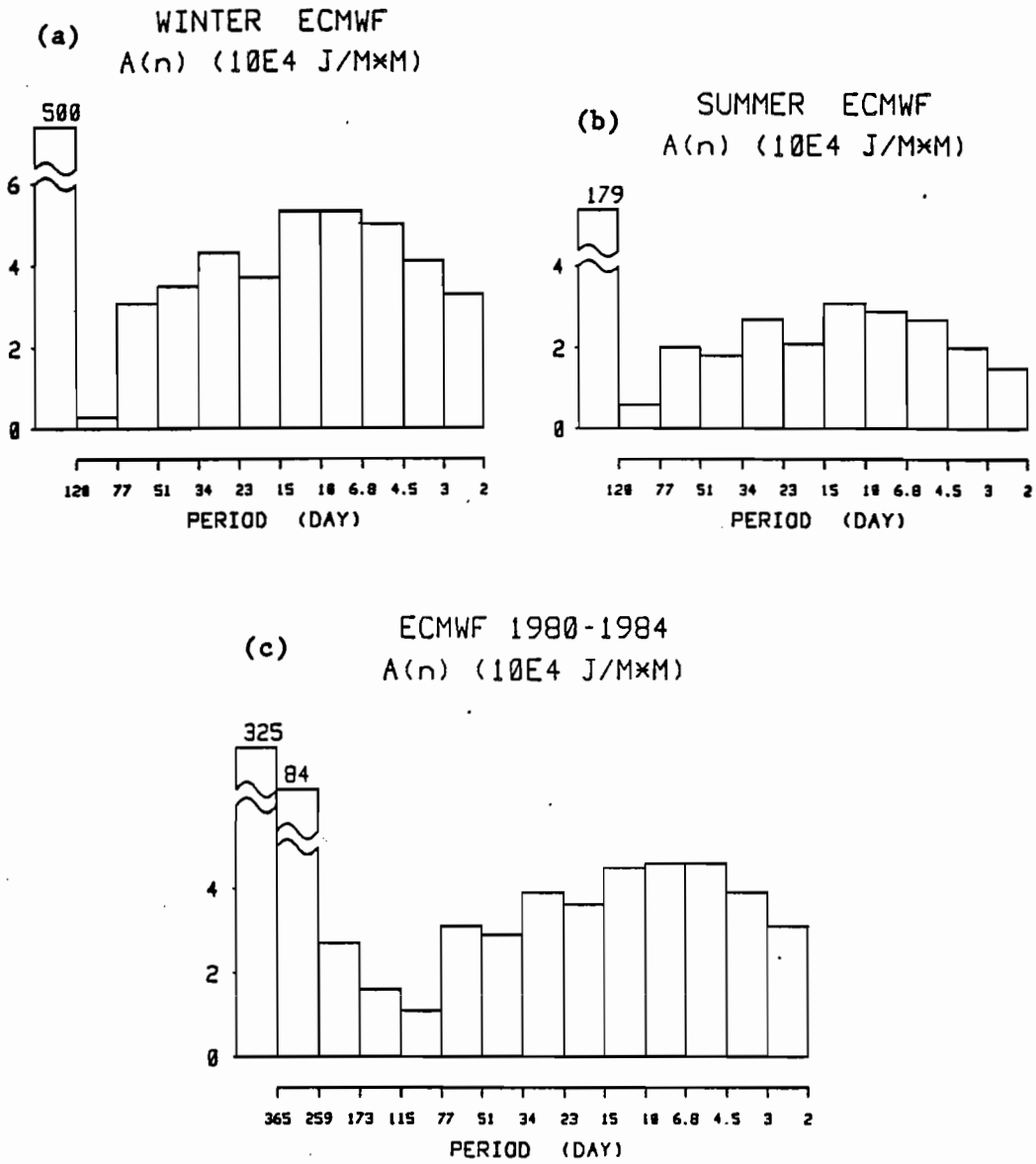


Fig. 2 As in Fig. 1, but for APE.

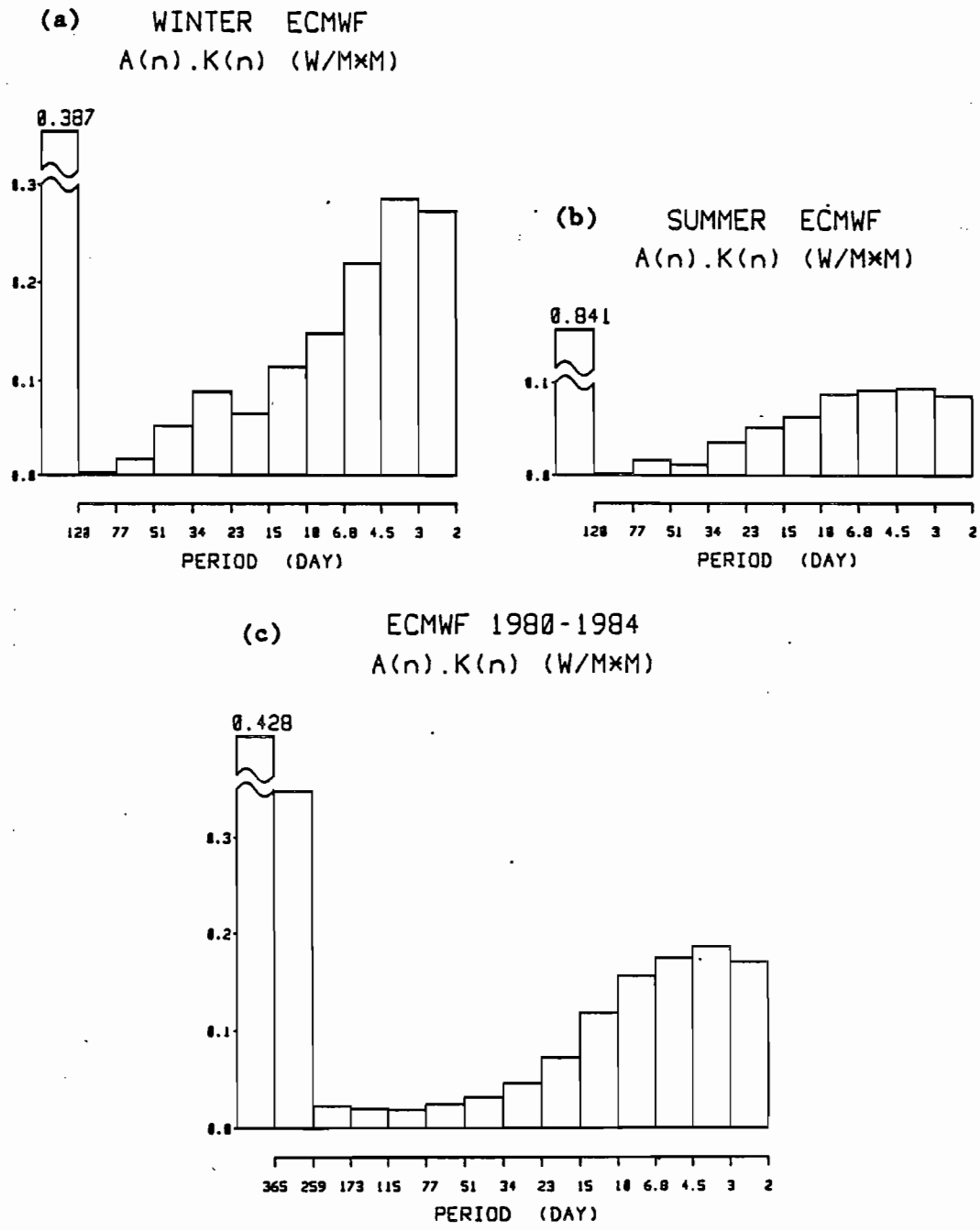


Fig. 3 As in Fig. 1, but for baroclinic conversion term. In units of W/m^2 .

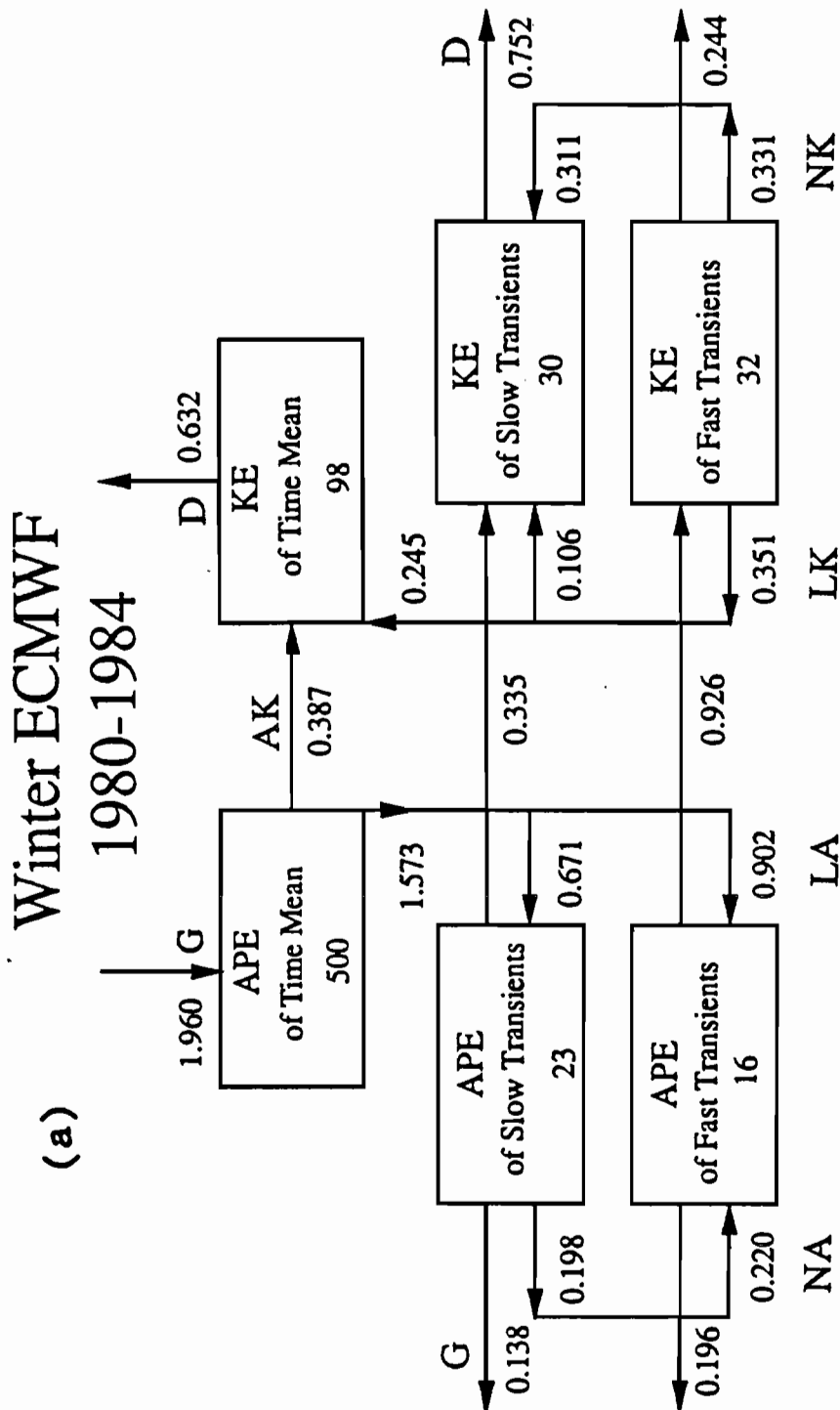
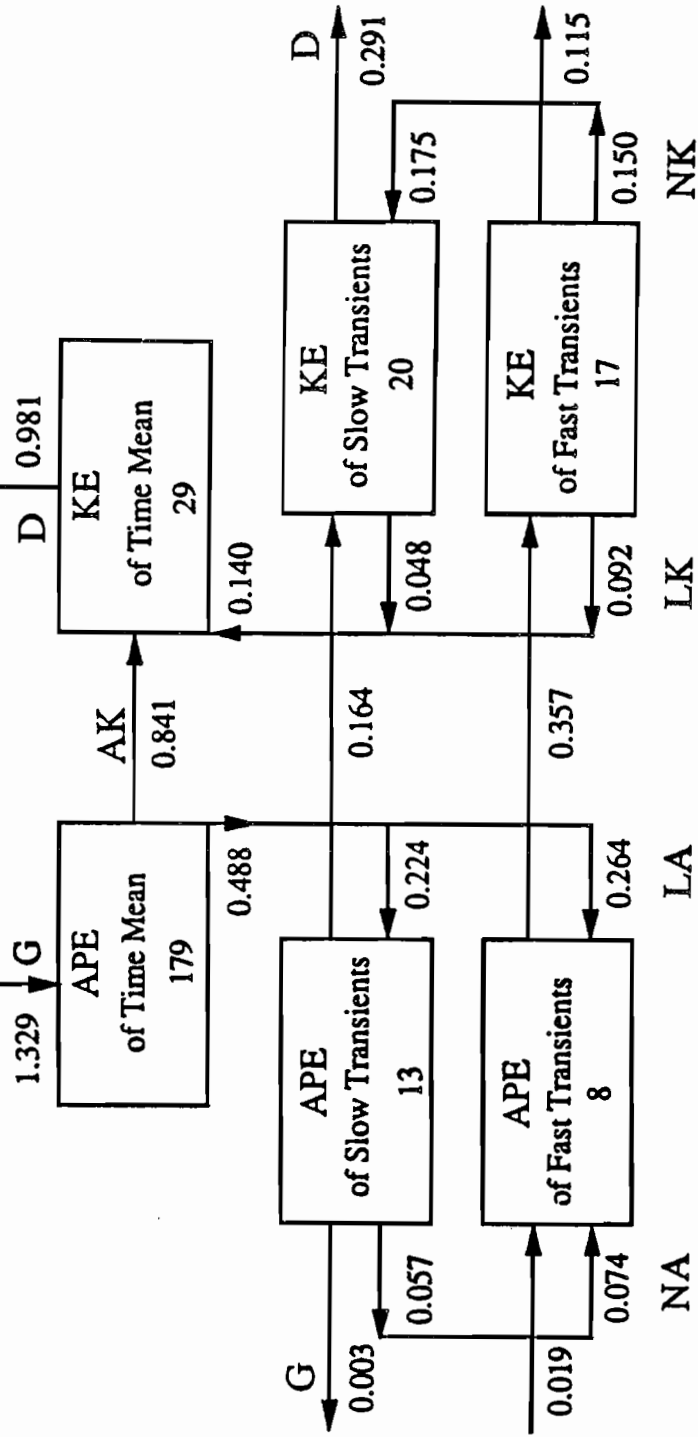


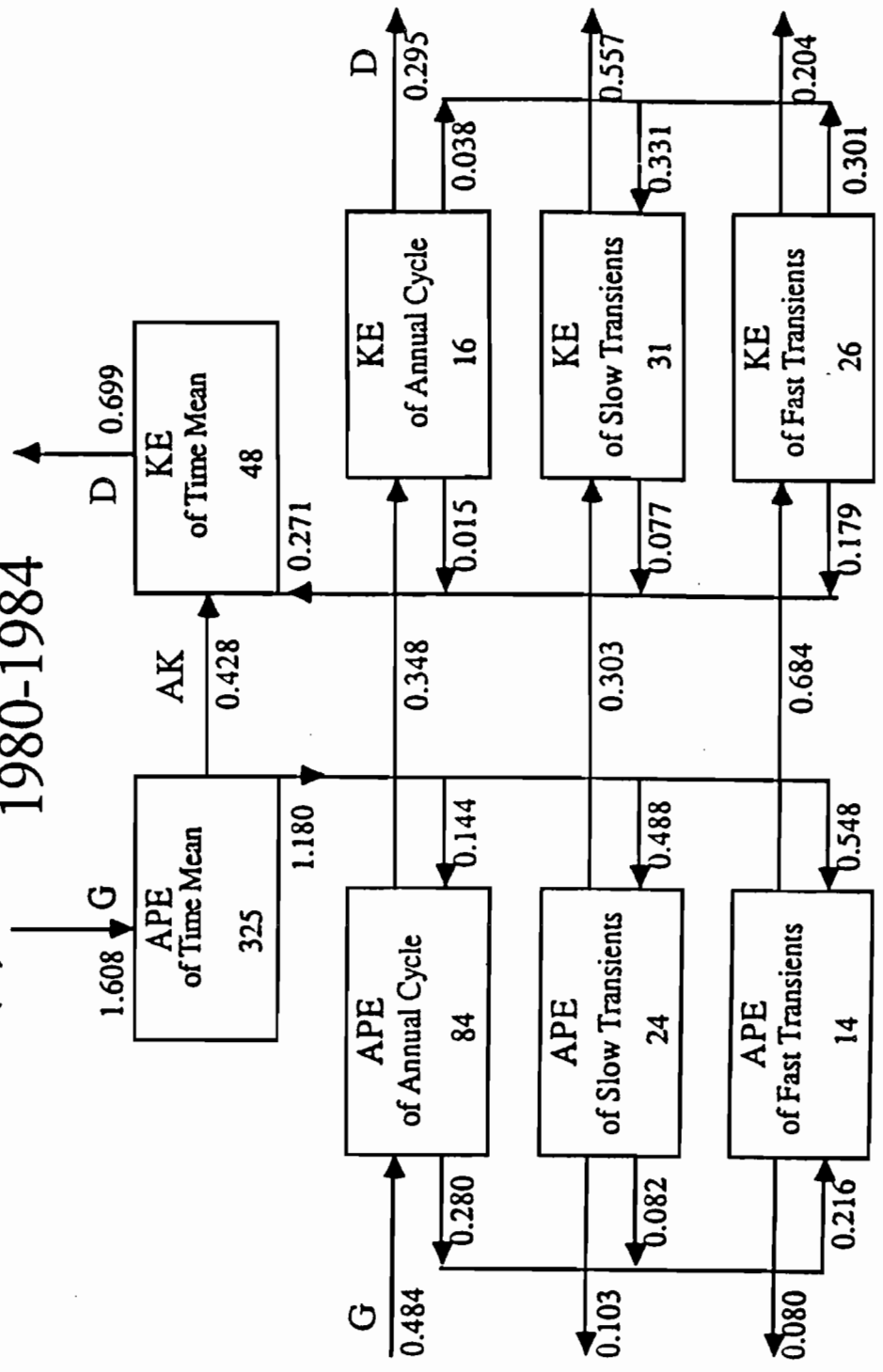
Fig. 4 Schematic depiction of the atmospheric energy cycle in the frequency domain. Numbers in boxes denote the energy storage in units of 10^4 J/m^2 , and fluxes of energy in W/m^2 . For (a) winter, (b) summer and (c) annual mean.

(b) Summer ECMWF
1980-1983



ECMWF 1980-1984

(c)



NA

LA

LK

NK

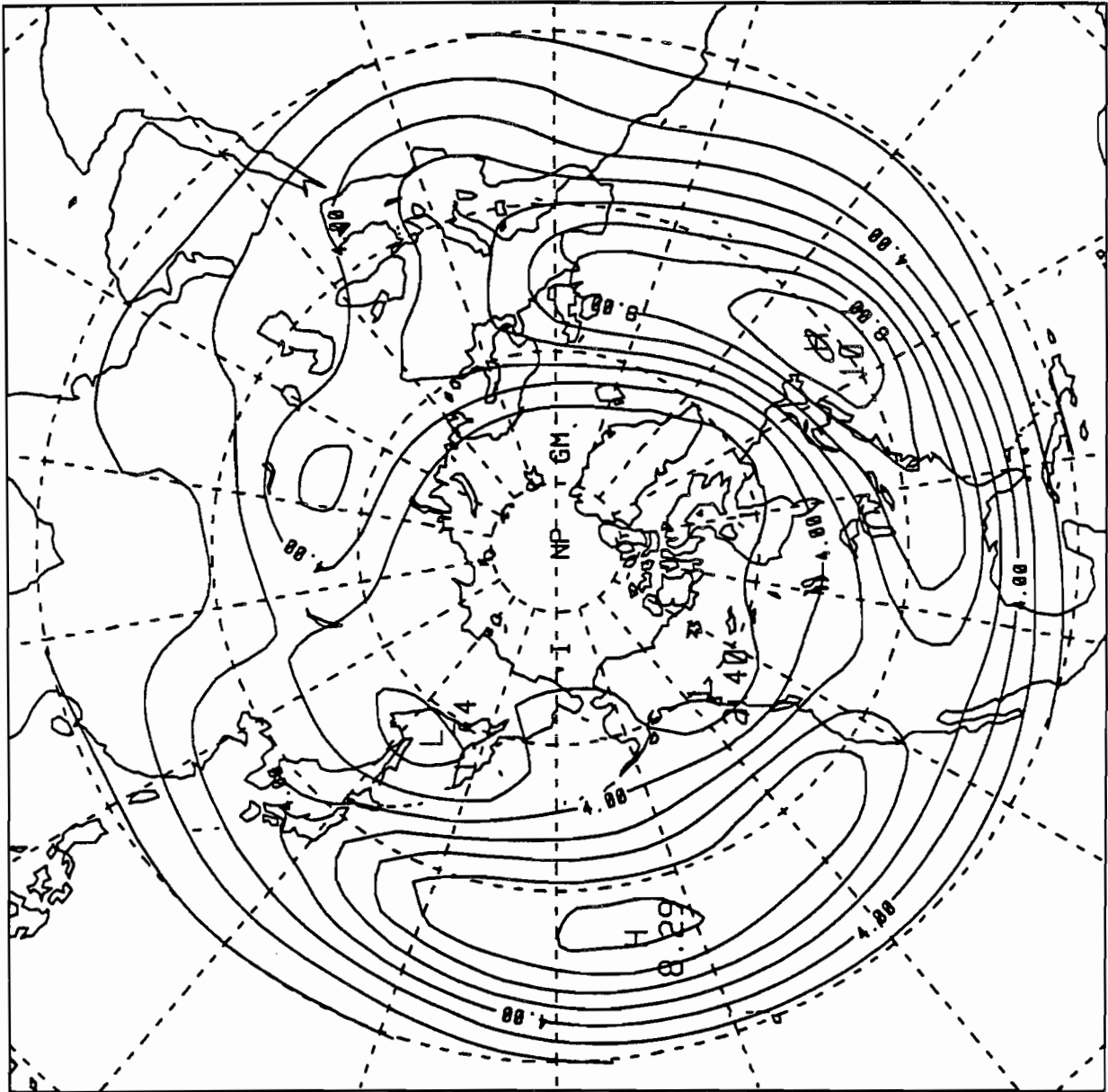


Fig. 5 Winter ECMWF high frequency KE. Vertically integrated with contour interval 10^5 J/m^2 .

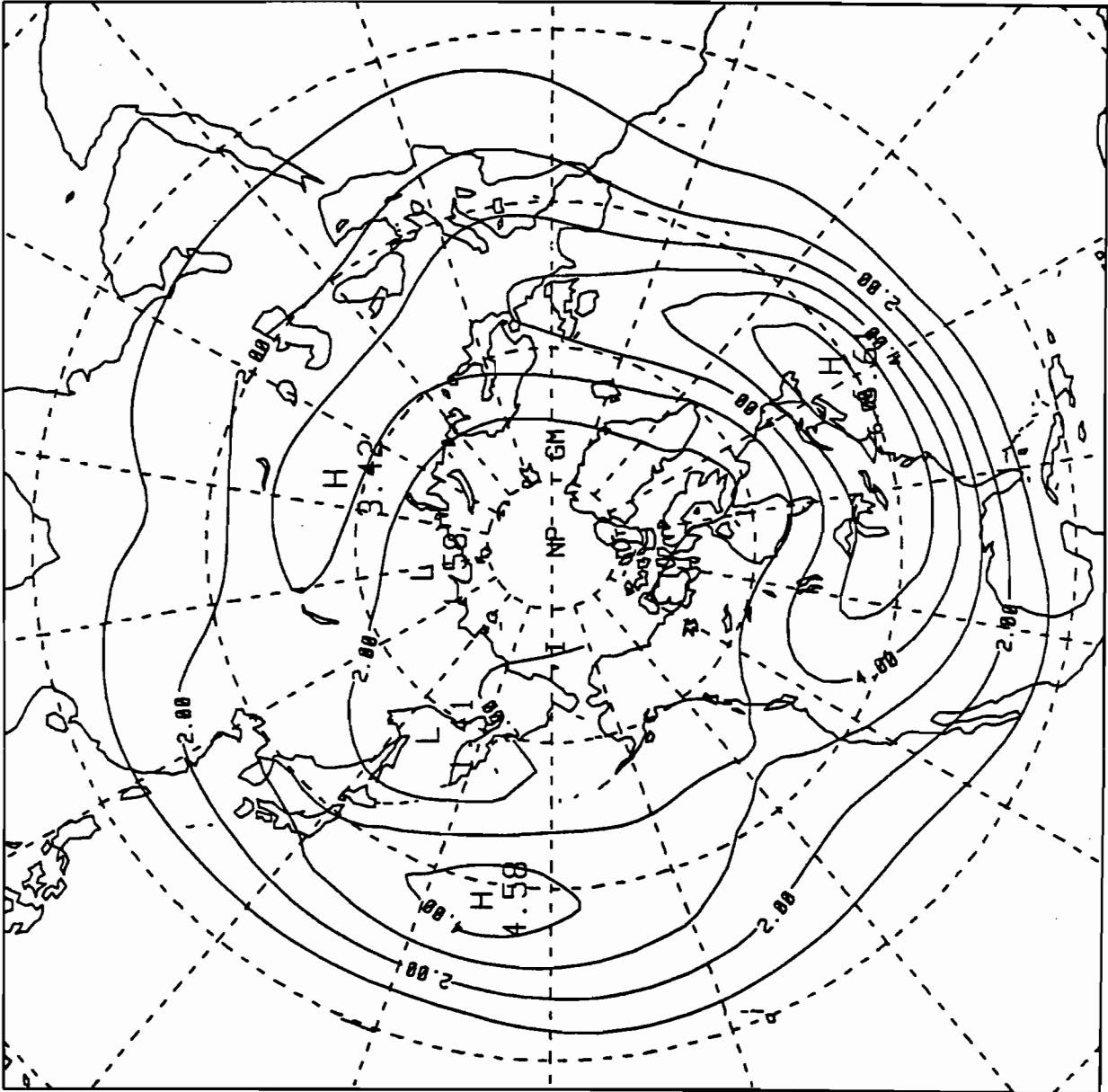


Fig. 6 Winter ECMWF high frequency APE. Vertically integrated with contour interval 10^5 J/m^2 .

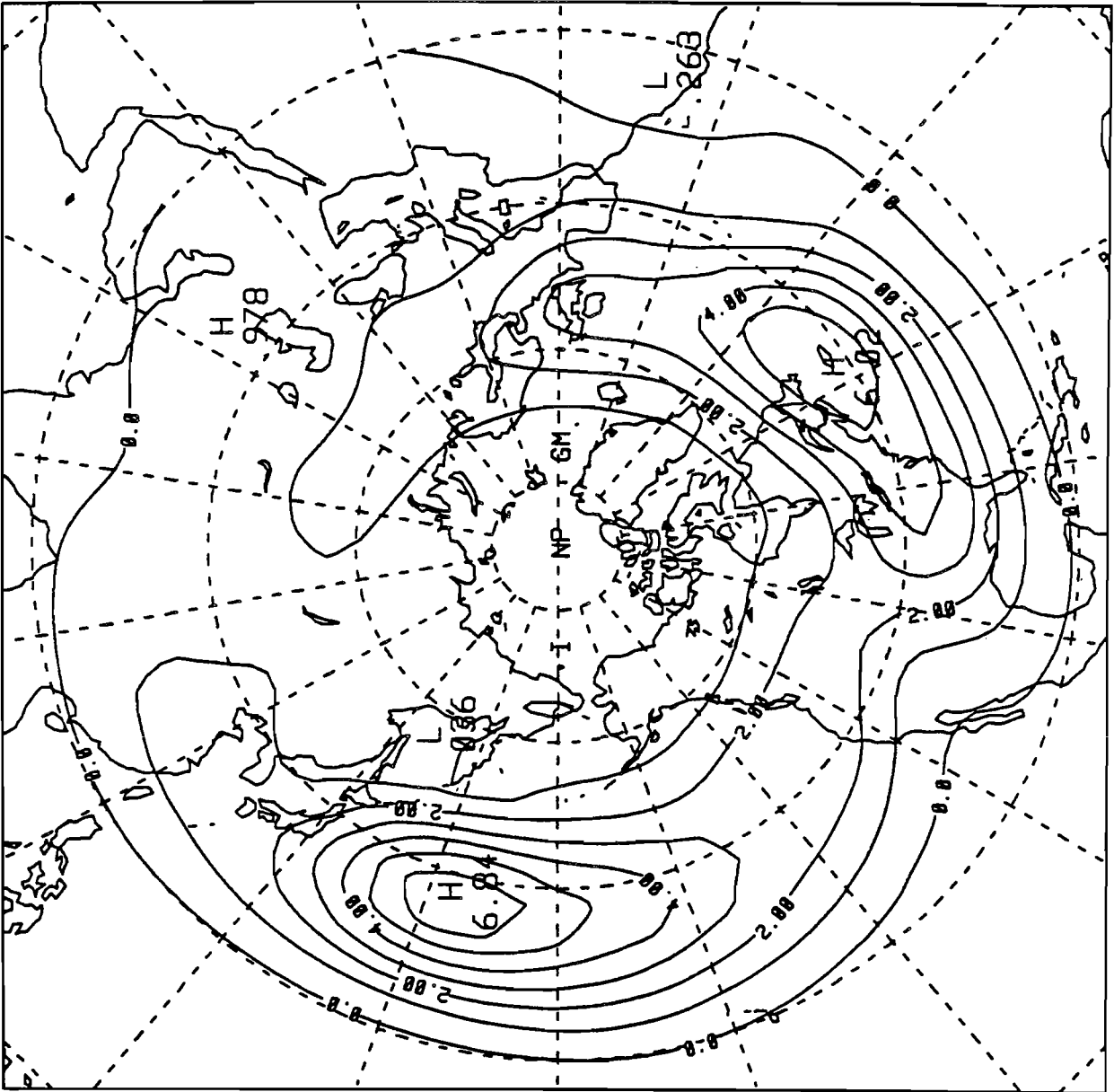


Fig. 7 Winter ECMWF high frequency AK. Vertically integrated with contour interval $1.0 W/m^2$.

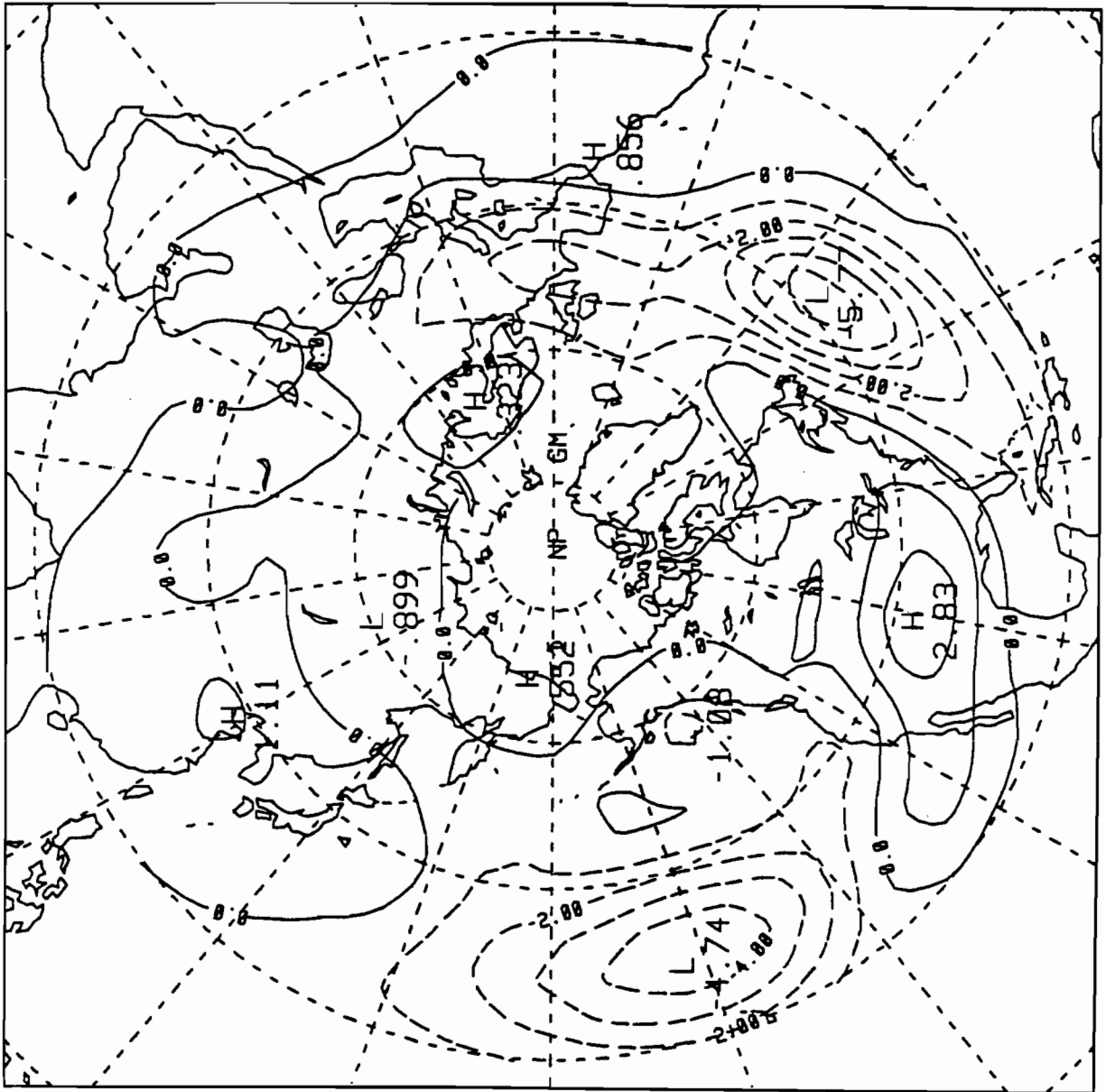


Fig. 8 Winter ECMWF high frequency LK. Vertically integrated with contour interval 1.0 W/m^2 .

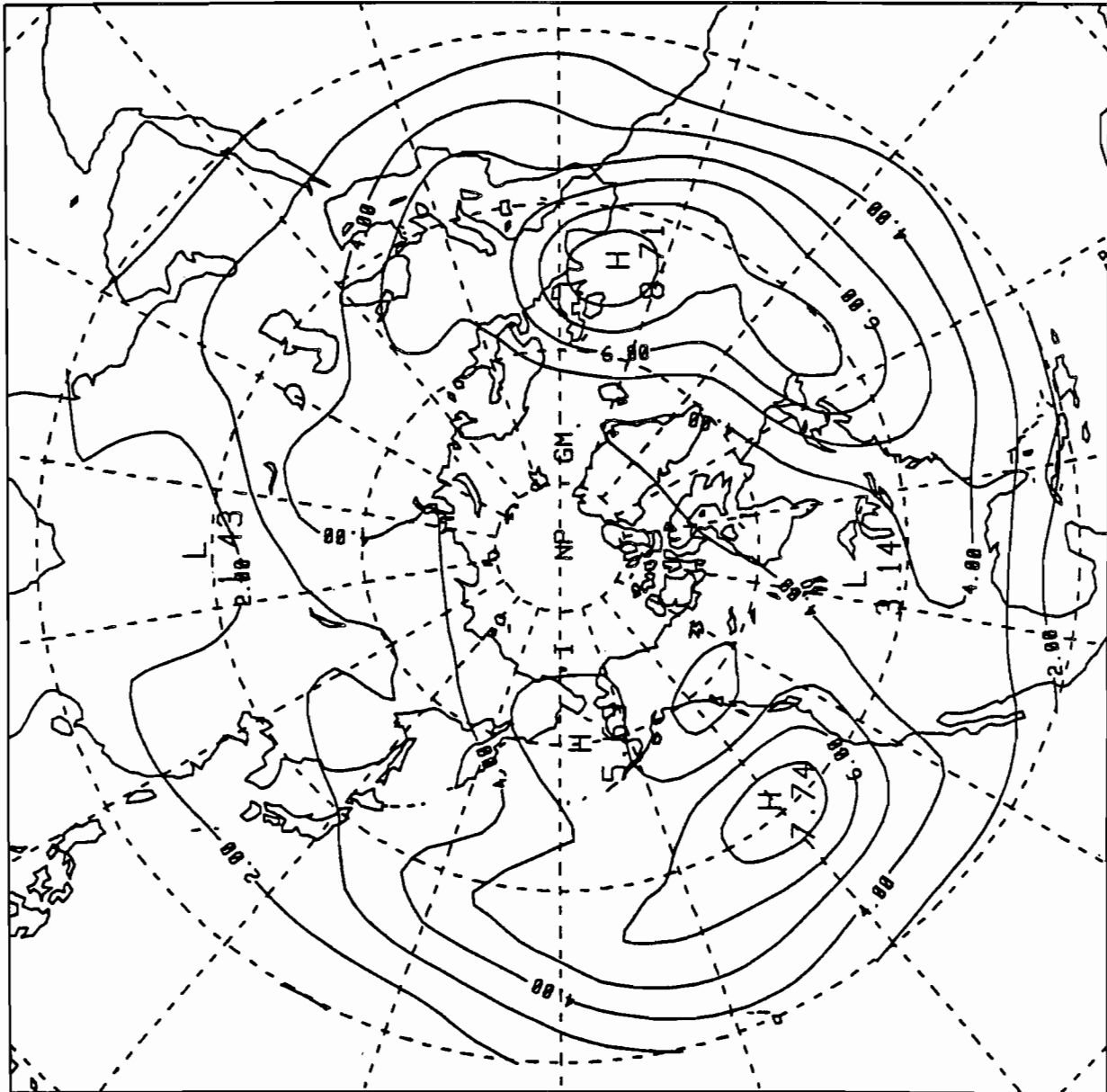


Fig. 9 Winter ECMWF low frequency KE. Vertically integrated with contour interval 10^5 J/m^2 .

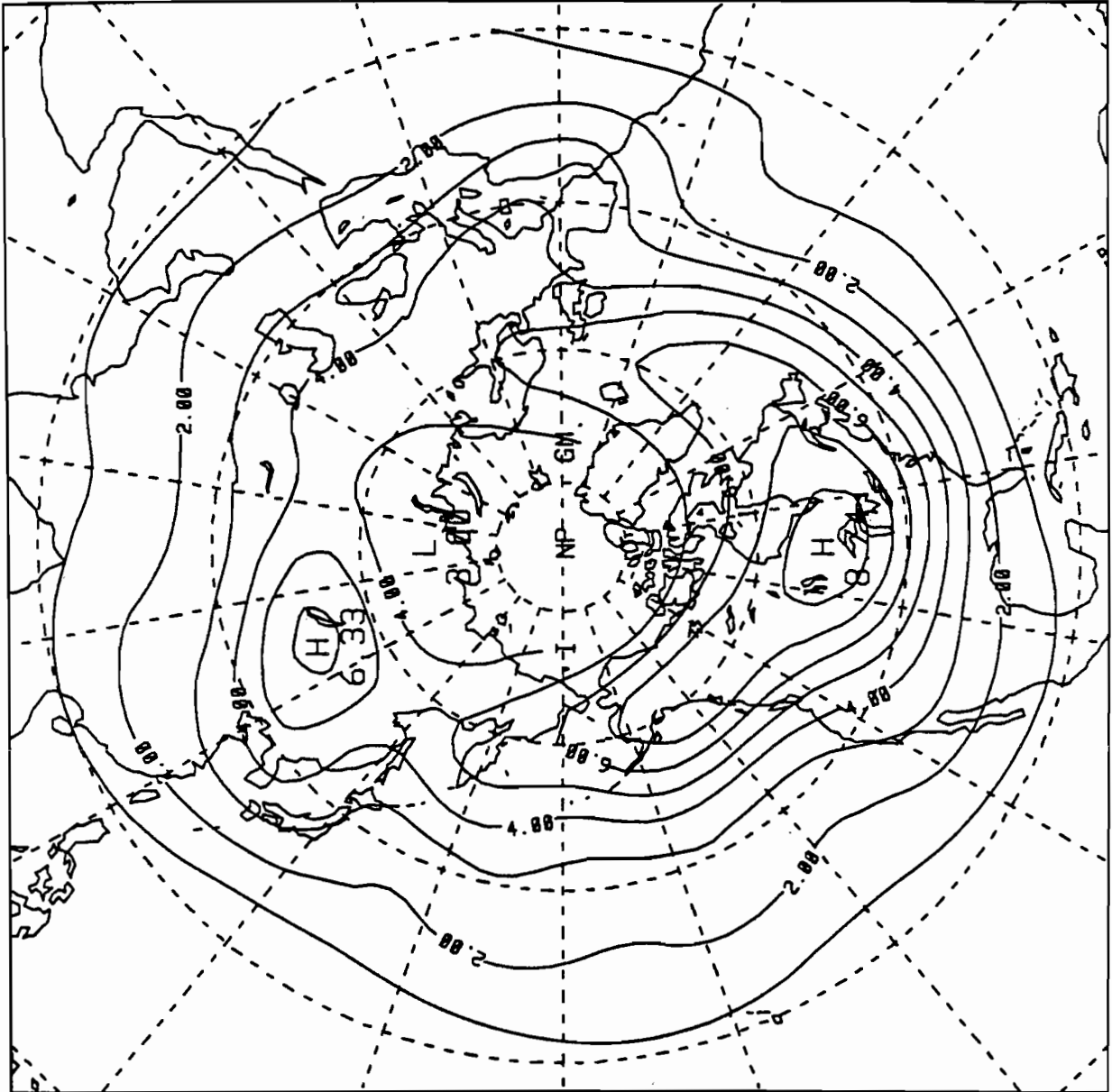


Fig. 10 Winter ECMWF low frequency APE. Vertically integrated with contour interval 10^5 J/m^2 .

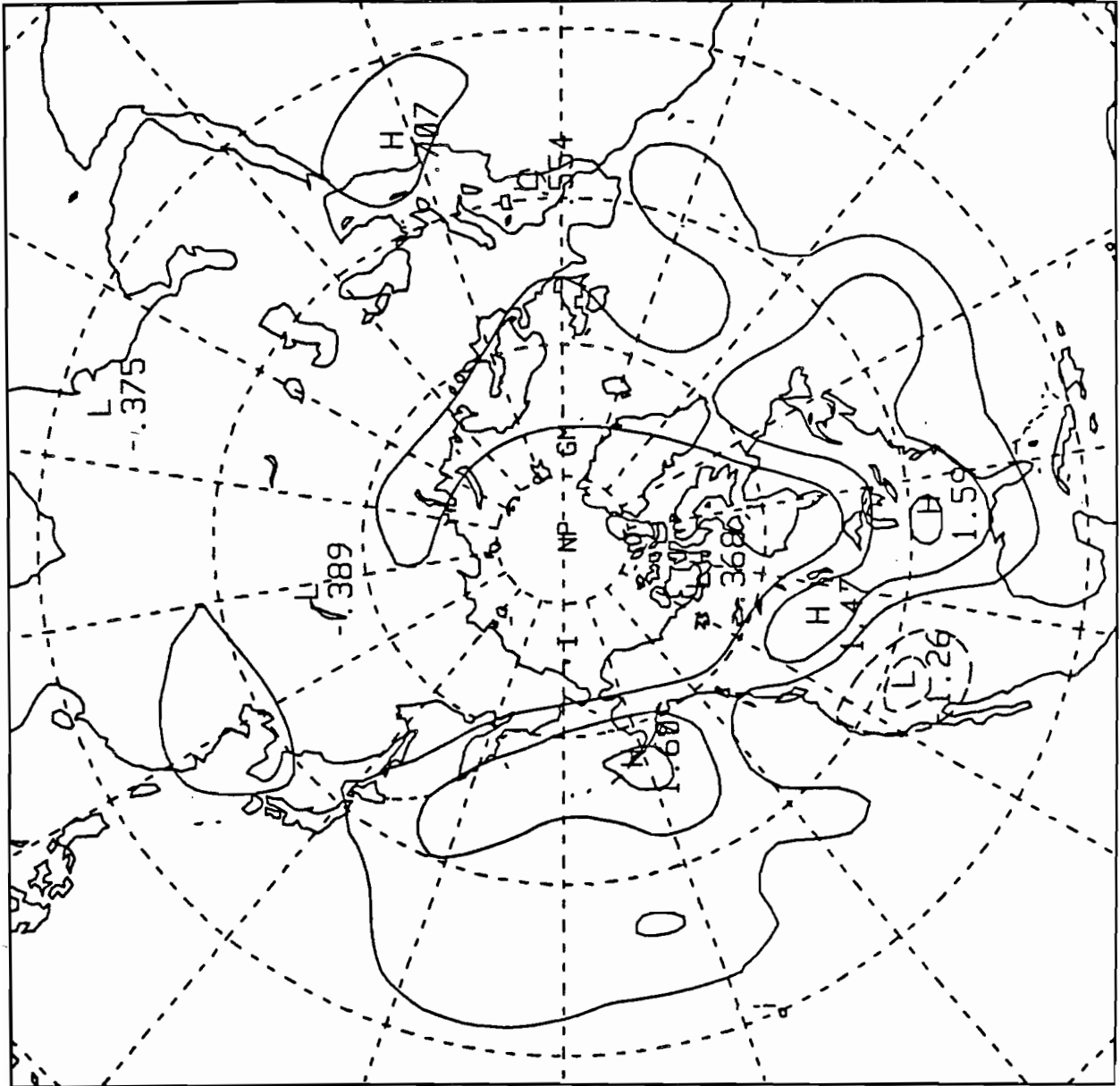


Fig. 11 Winter ECMWF low frequency AK. Vertically integrated with contour interval $0.5 W/m^2$.

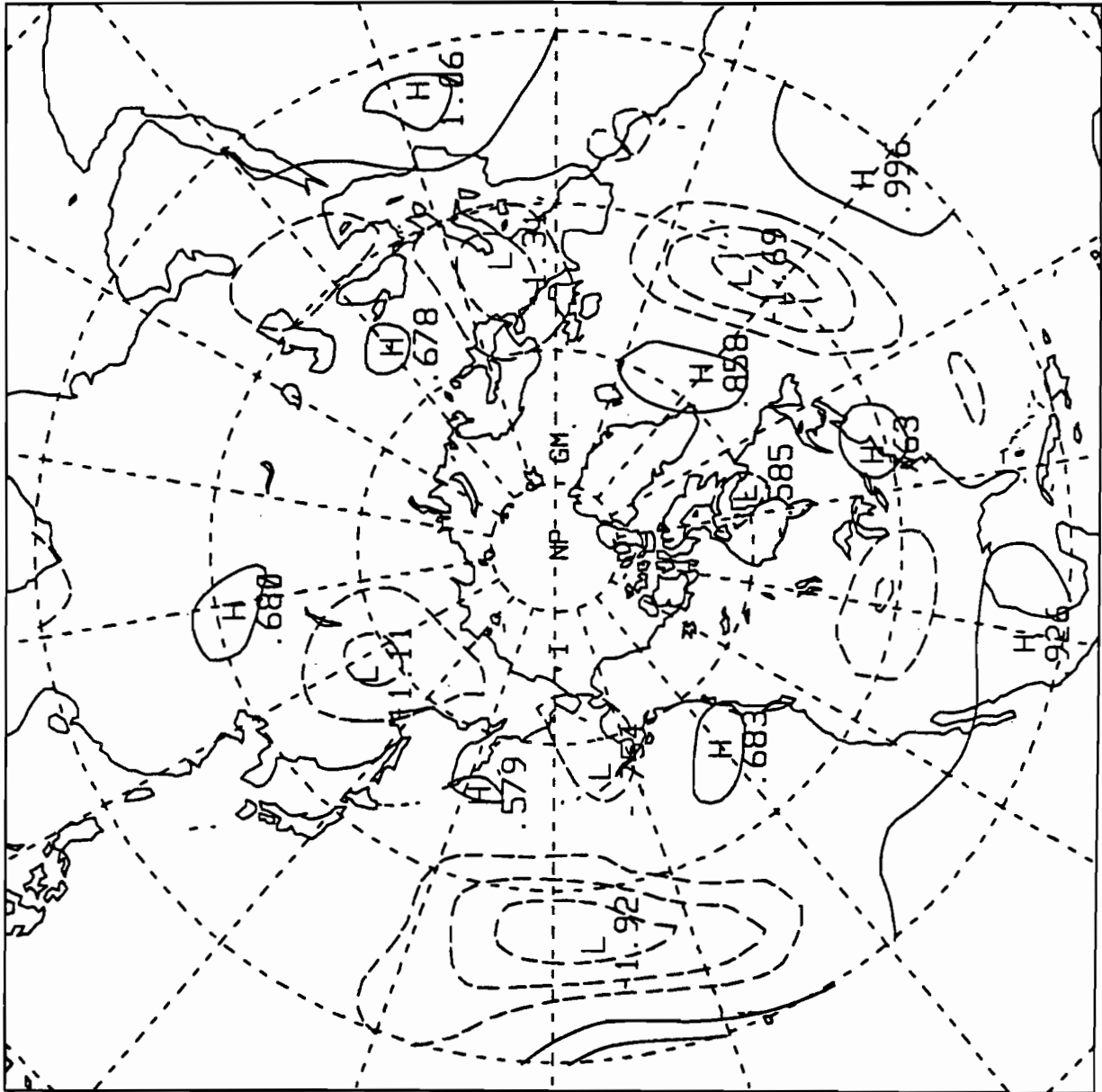


Fig. 12 Winter ECMWF low frequency BT. Vertically integrated with contour interval 0.5 W/m².

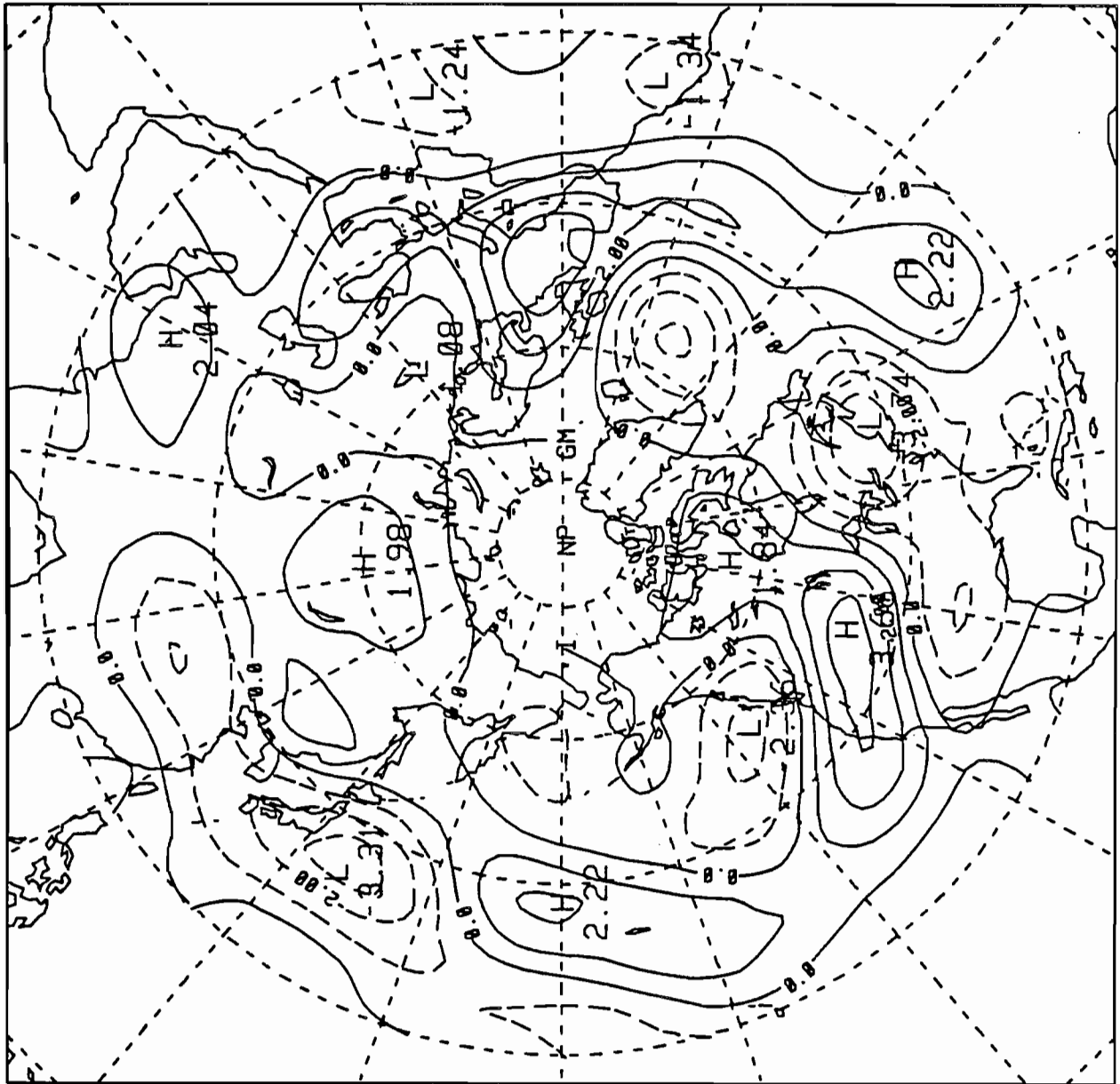


Fig. 13 Winter ECMWF low frequency LK. Vertically integrated with contour interval 1.0 W/m^2 .

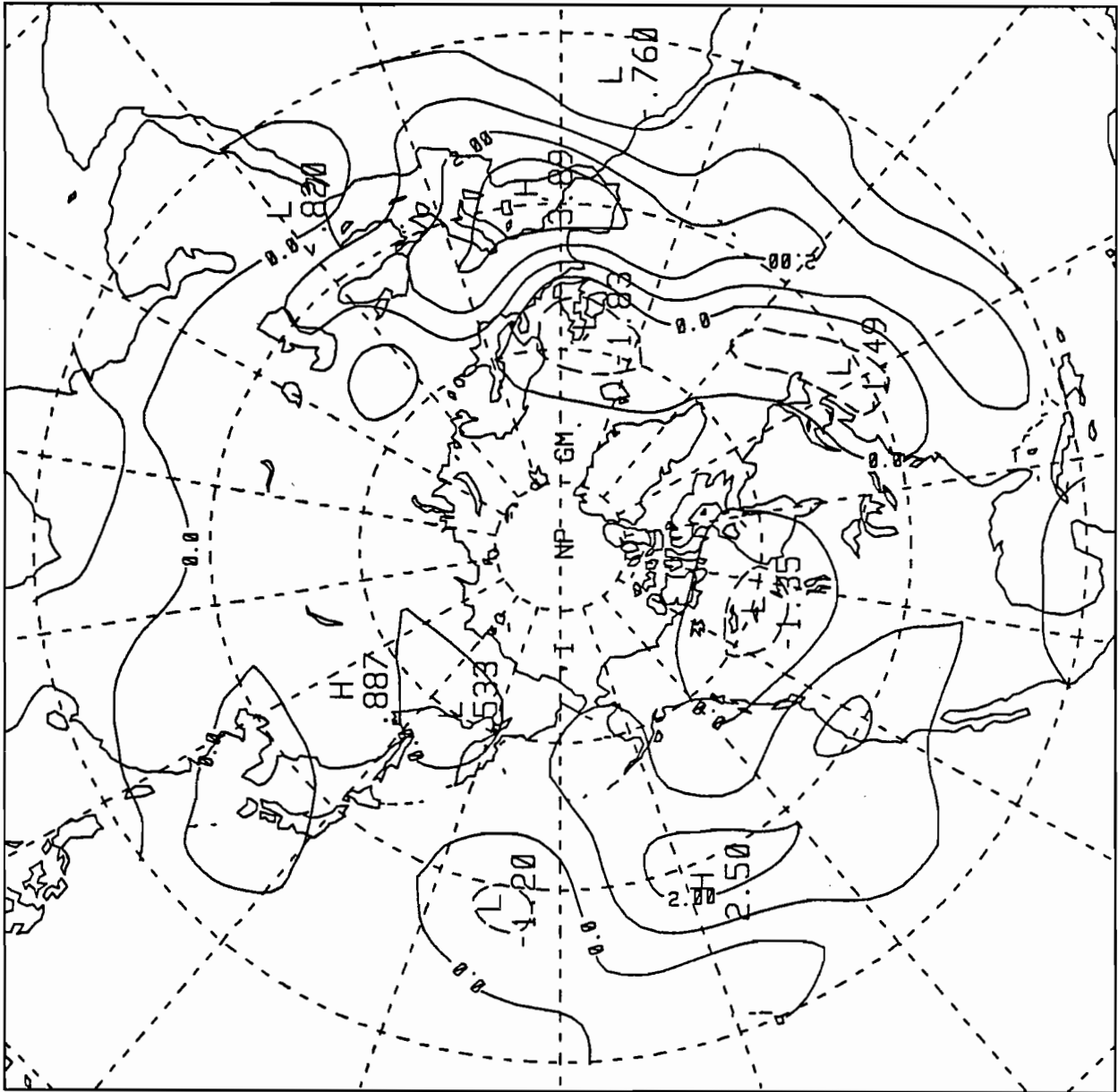


Fig. 14 Winter ECMWF low frequency NK. Vertically integrated with contour interval 1.0 W/m².

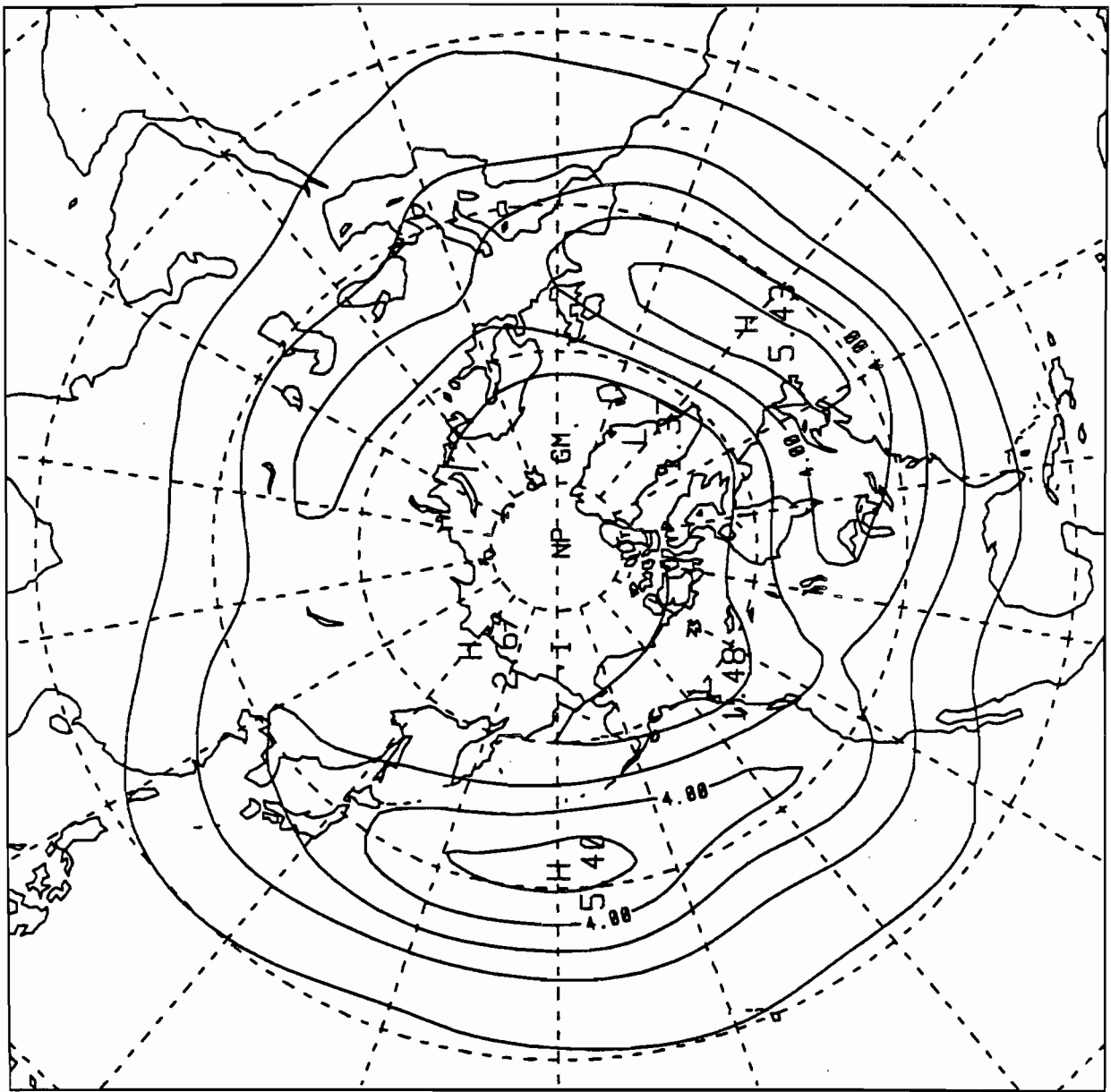


Fig. 15 Summer ECMWF high frequency KE. Vertically integrated with contour interval 10^5 J/m^2 .

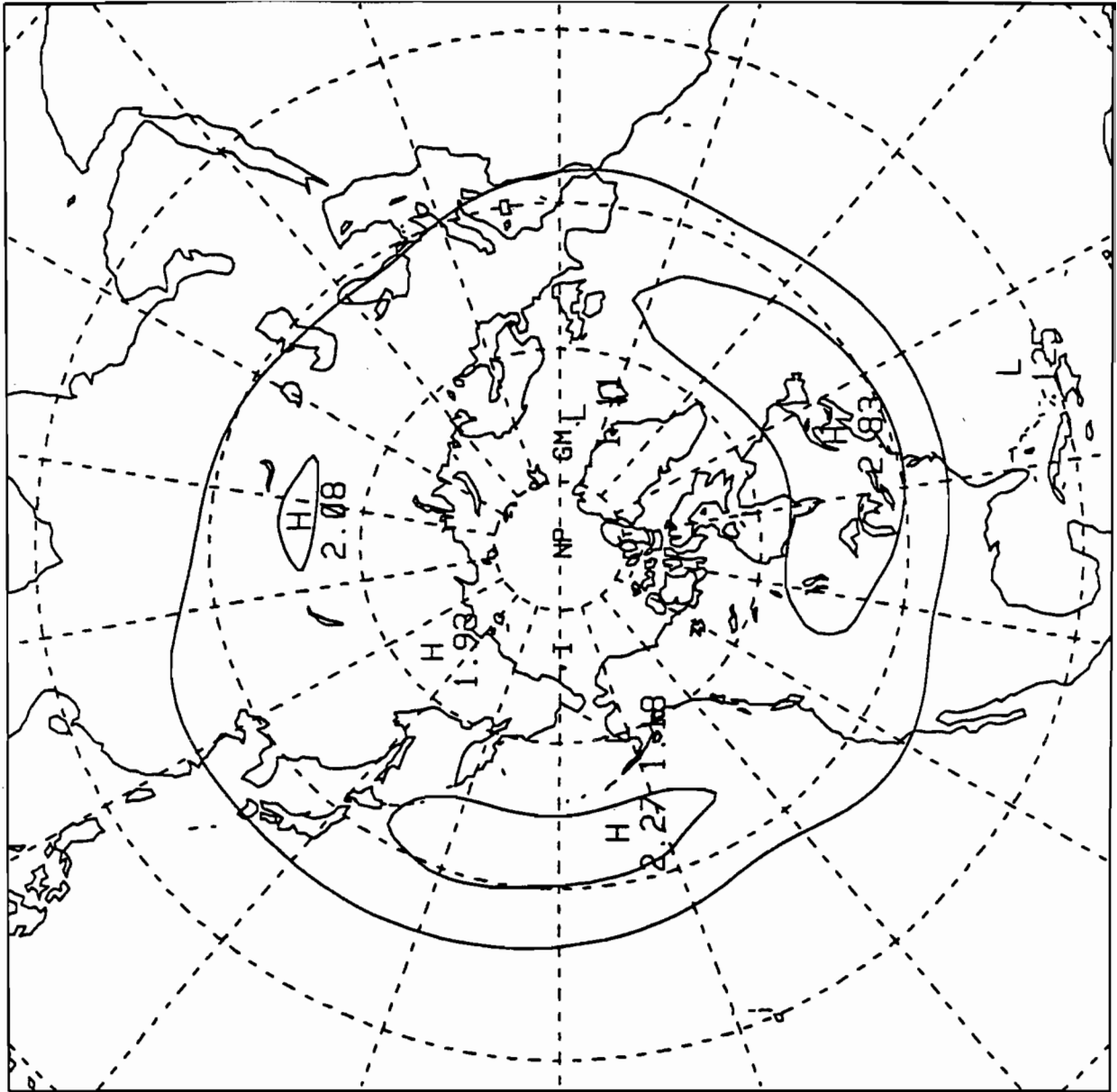


Fig. 16 Summer ECMWF high frequency APE. Vertically integrated with contour interval 10^5 J/m^2 .

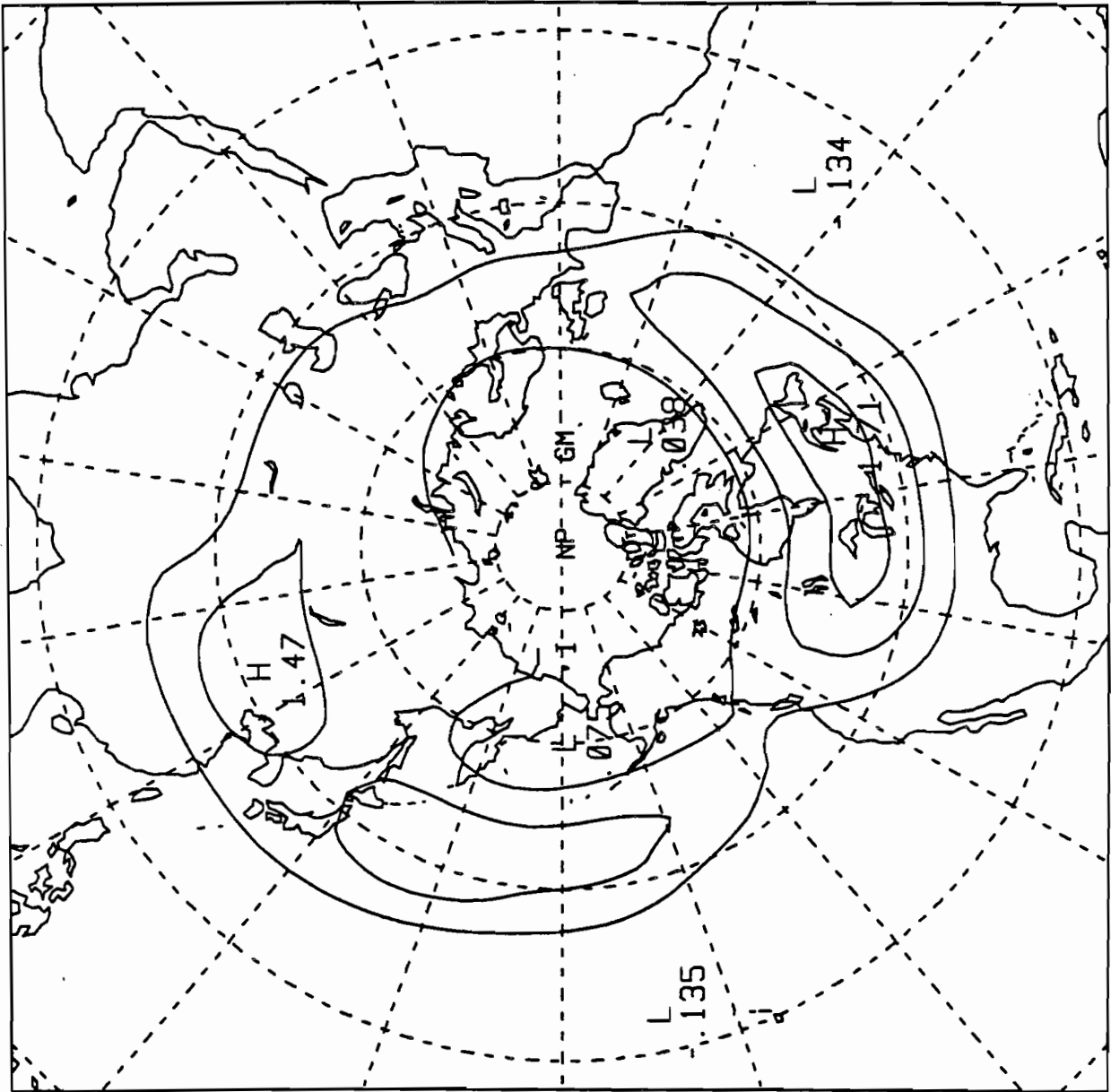


Fig. 17 Summer ECMWF high frequency AK. Vertically integrated with contour interval 0.5 W/m^2 .

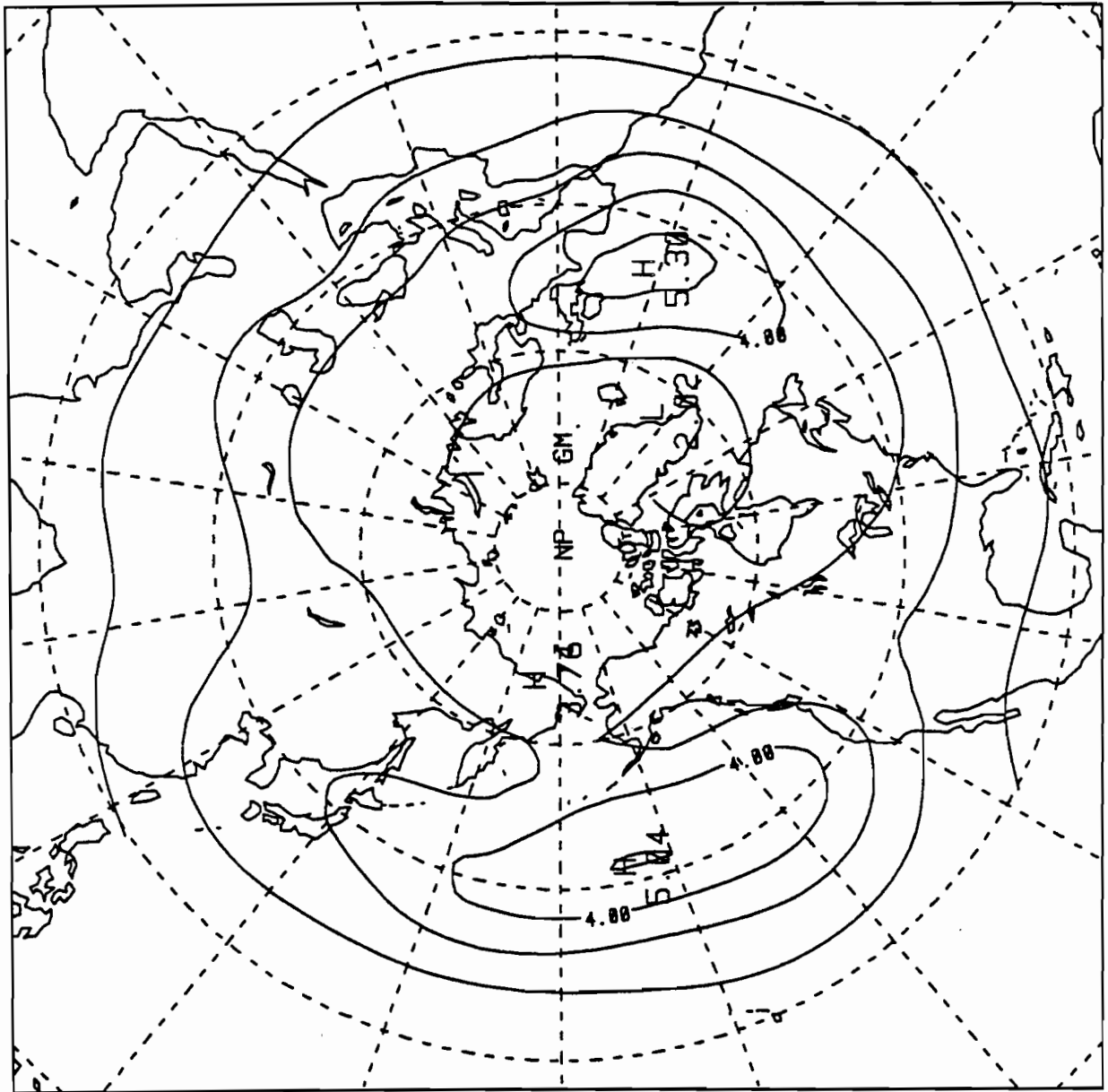


Fig. 18 Summer ECMWF low frequency KE. Vertically integrated with contour interval 10^5 J/m^2 .

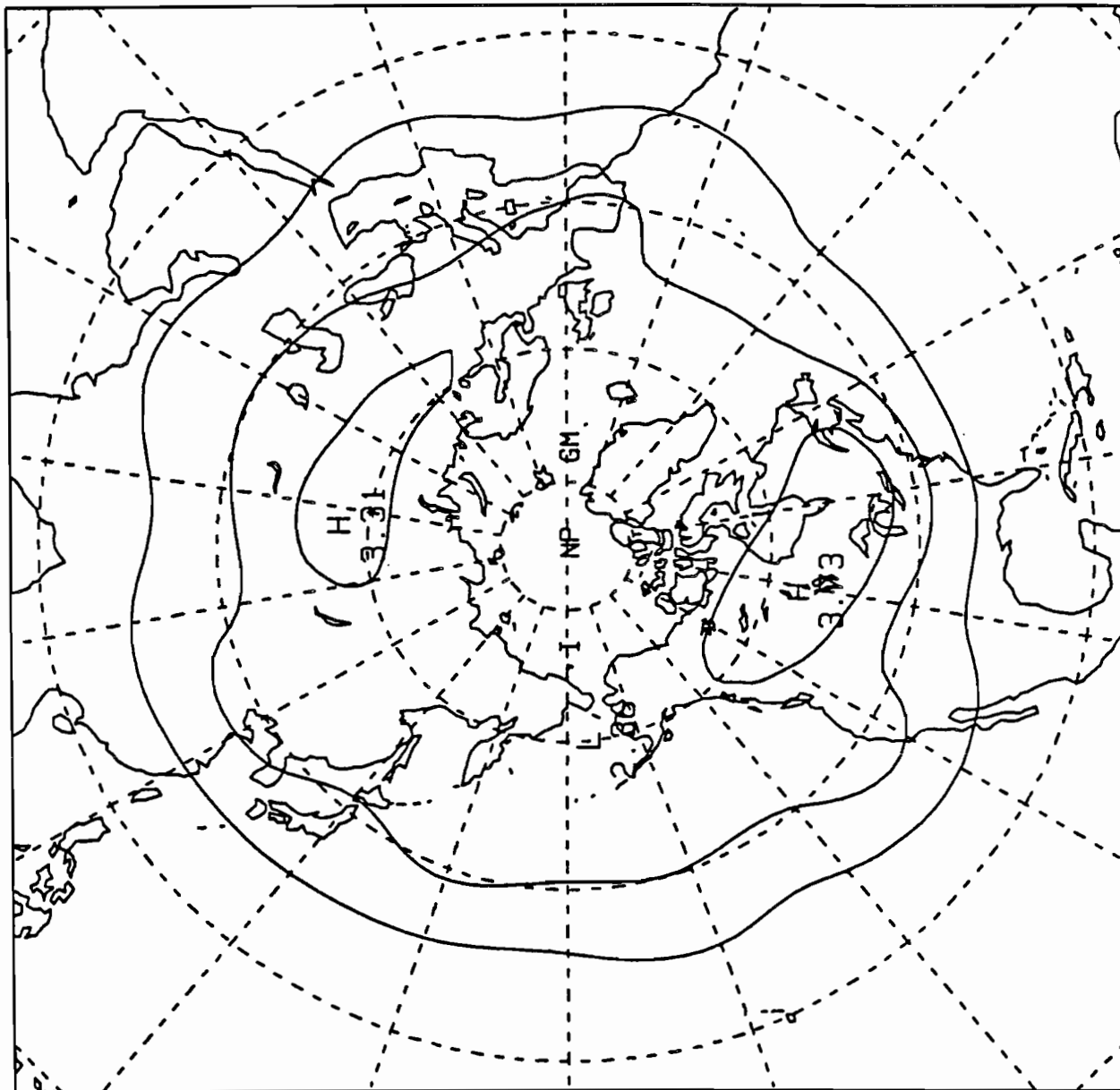


Fig. 19 Summer ECMWF low frequency APE. Vertically integrated with contour interval 10^5 J/m^2 .

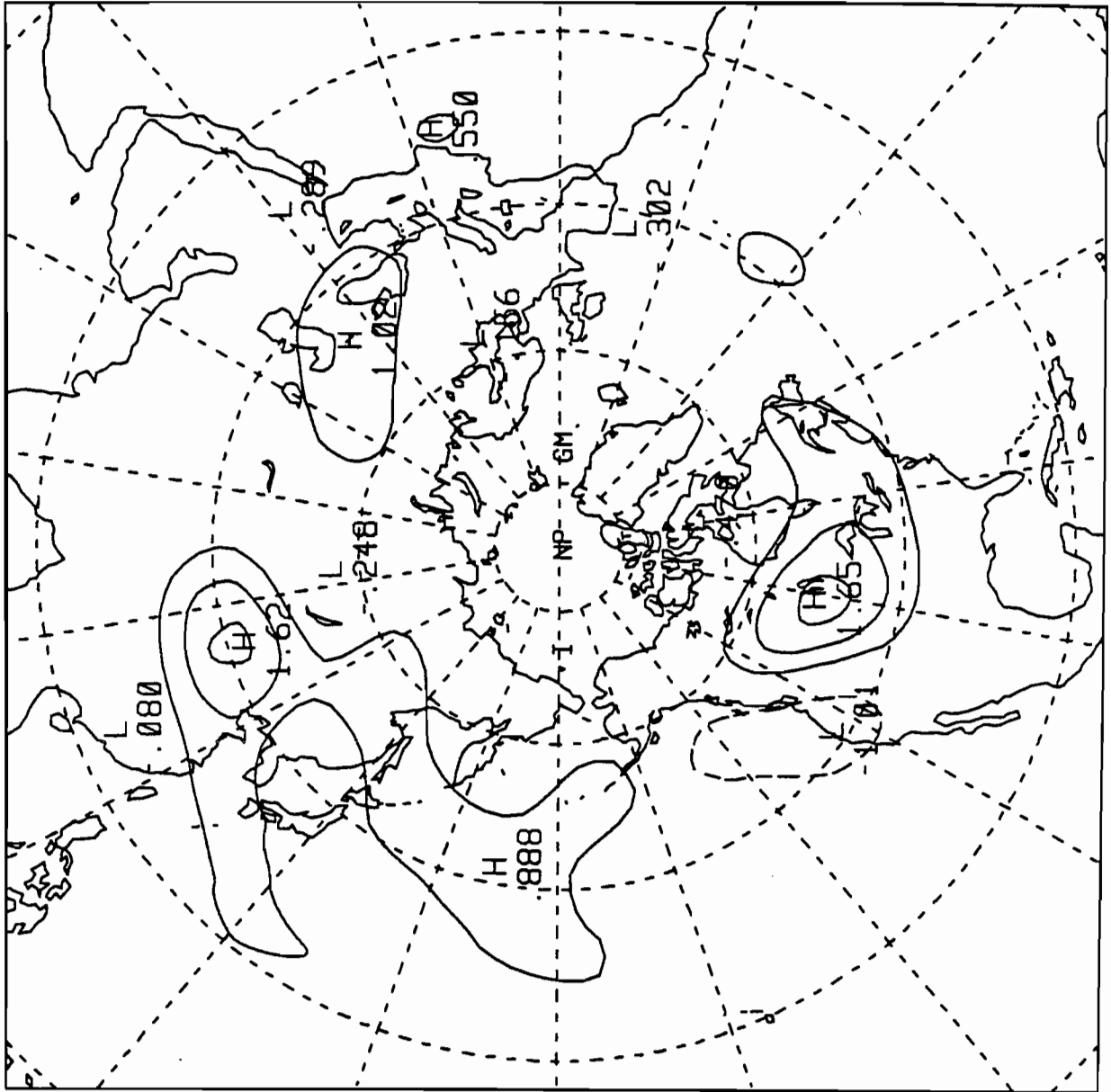


Fig. 20 Summer ECMWF low frequency AK. Vertically integrated with contour interval 0.5 W/m^2 .

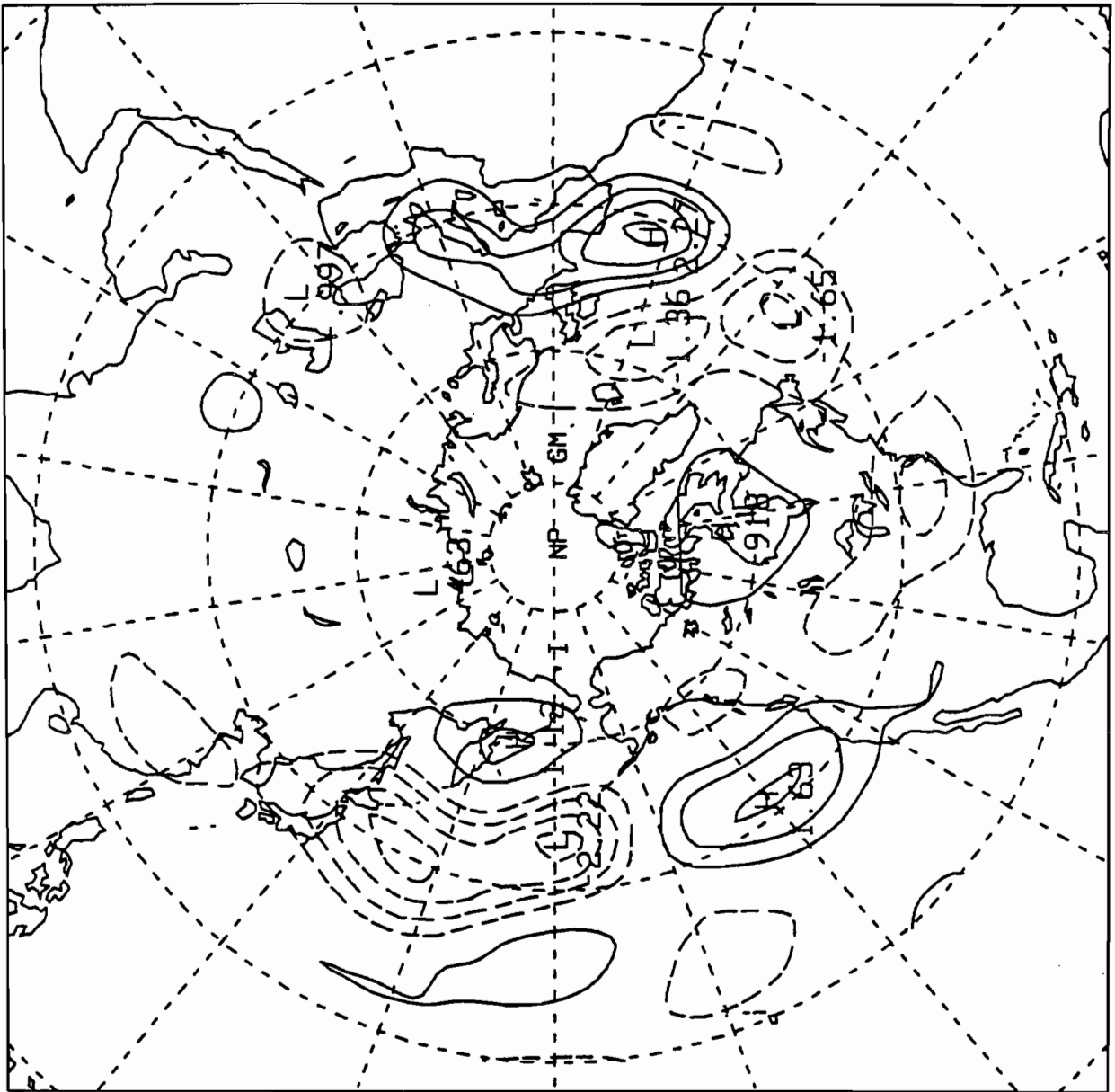


Fig. 21 Summer ECMWF low frequency LK. Vertically integrated with contour interval 0.5 W/m^2 .

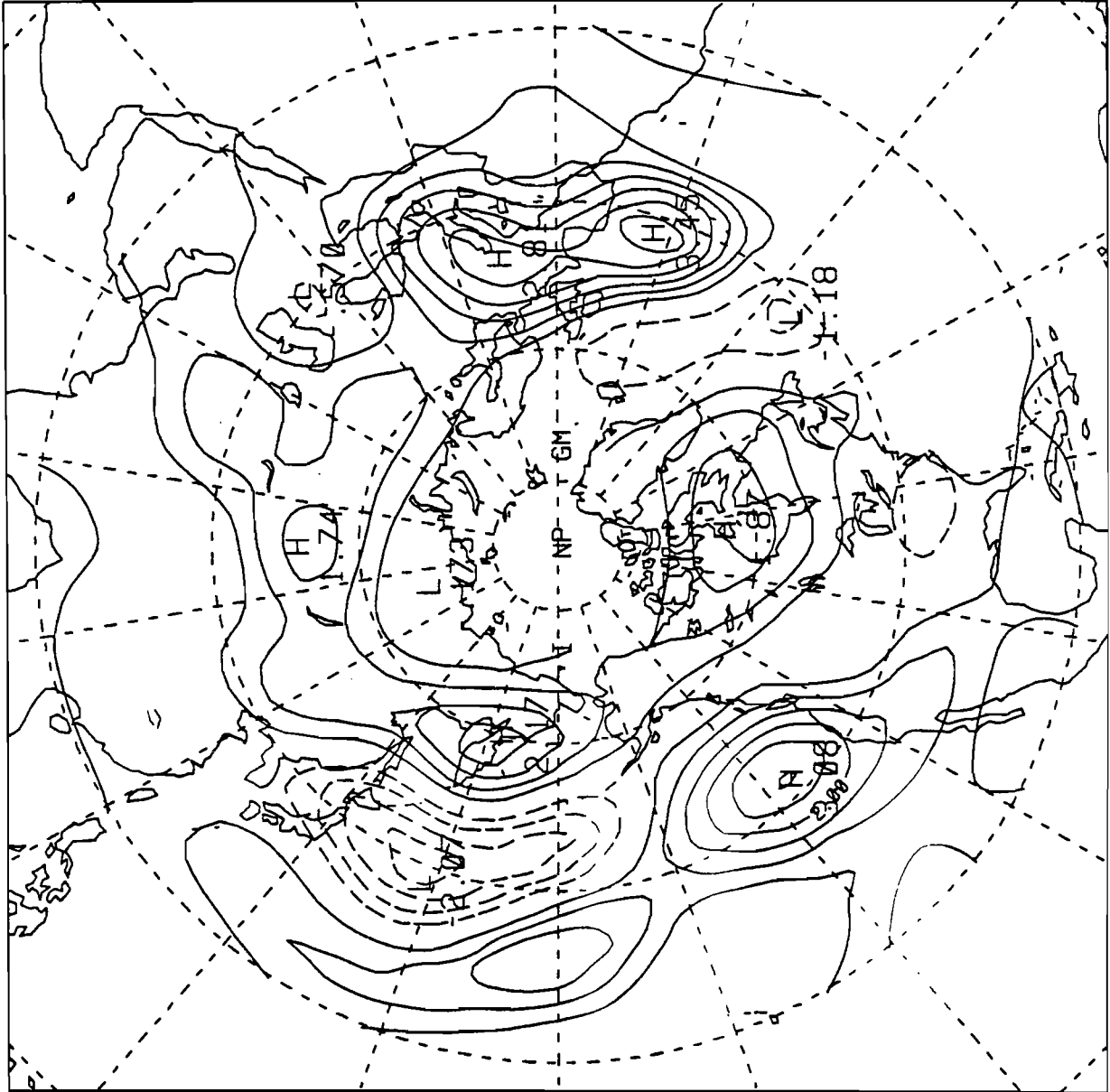


Fig. 22 Summer ECMWF low frequency LK + NK. Vertically integrated with contour interval 0.5 W/m^2 .

